UNITED STATES DEPARTMENT OF THE INTERIOR

GEOLOGICAL SURVEY

The application of uranium-thorium systematics to rocks from the Lassen Dome Field, California

Deborah A. Trimble, Michael A. Clynne,

and Stephen W. Robinson[1]

Open-File Report 84-371

[1]Menlo Park, Ca.

1984

TABLE OF CONTENTS

TABLE OF CONTENTS--Continued

TABLE OF CONTENTS--Continued

LIST OF ILLUSTRATIONS

LIST OF ILLUSTRATIONS--Continued

LIST OF TABLES

ABSTRACT

^{238}U-^{230}Th disequilibrium systematics were applied to a suite of fifteen dacites, rhyodacites, and mafic inclusions from the Lassen dome field, Lassen Volcanic National Park, California. Chemical procedures were established and are reported for separation and purification of uranium and thorium from whole-rock samples and mineral separates. Activities of ^{230}Th, ^{232}Th, ^{234}U, and ^{238}U were determined by alpha spectrometry.

Age determinations were made for five of the rhyodacite units using ^{230}Th-^{238}U isochrons. The determined ages range from 3,600 to 57,000 years, and are in agreement with volcanic and glacial stratigraphy and with preliminary radiocarbon and K-Ar ages.

The rocks from the Lassen dome field have ($^{230}Th/^{238}U$) ratios greater than 1, with few exceptions, and plot on a ^{230}Th-^{238}U isochron diagram in a field close to that of ocean island basalts. The observed enrichment in thorium relative to uranium in the majority of the rocks from the Lassen region is the result of partial melting events. The linear relationship that exists between uranium and thorium abundances and the constant Th/U ratios with increasing SiO_2 content indicate that rocks of the Lassen dome field are genetically related to other rocks of the Lassen Volcanic Center by fractional crystallization. Th/U ratio values lower than 3.7 and ($^{238}U/^{232}Th$) ratios greater than 0.81

suggest that the mantle source for the rocks of the Lassen dome field has been depleted by previous partial melting events. Low concentrations of uranium (0.5 - 3.75 ppm) and thorium (1.4 - 11.1 ppm) indicate that assimilation of crustal material is not a sigificant process in the origin of the magmas of the Lassen Volcanic Center. An enrichment of uranium relative to thorium in pyroclastic rocks and their associated volcanic domes suggests that uranium transport in a gaseous complex may be important in the magmatic system.

The data support a origin for the intermediate and silicic rocks of the Lassen Volcanic Center by fractional crystallization of mantle derived mafic magmas in an open system.

INTRODUCTION

The relationships among decay products of uranium and thorium provide a method of dating materials from approximately 10,000 to 300,000 years old. U/Th systematics can be applied to a variety of natural materials including deep sea sediment, lake sediment, carbonate, water, bone, and igneous rocks.

This study was undertaken to apply U/Th disequilbrium systematics to the study of young, silicic volcanic rocks from the Lassen Volcanic Center, California.

Historical Background

Cerrai and others (1965) were the first to propose dating young volcanic rocks using U/Th systematics. They used zircon and ilmenite extracted from beach sand collected south of Nettuno, Italy. These heavy minerals were assumed to be a natural concentration derived from volcanic tuffs in the immediate area. The aim of their study was to test the feasibility of the dating method rather than to obtain exact geologic ages.

Kigoshi (1967) dated samples of granite, pumice, and lava by measuring the excess ^{230}Th grown *in situ* from decay of ^{234}U since solidification. He reasoned that the ratio of ^{230}Th present at solidification to the ^{230}Th grown *in situ* varied in each mineral according to its uranium and thorium content. Therefore the

accumulated ^{230}Th is proportional to the amount of ^{234}U or ^{234}Th present in each mineral phase, and the initial ^{230}Th content is proportional to the amount of ^{232}Th. Kigoshi measured the activities of ^{230}Th, ^{232}Th, and ^{234}Th in each phase. Plotting these on a $^{230}Th/^{232}Th$ versus $^{234}Th/^{232}Th$ diagram he was able to obtain dates from the slope of the resulting line (isochron). The dates obtained agreed well with the known ages of the samples.

Taddeucci and others (1967) studied rhyolites from Mono Craters and Inyo Domes, California. They measured ^{238}U, ^{230}Th, and ^{232}Th in four different phases: quartz, glass, olivine, and hornblende. They concluded that the hornblende-glass pair had a sufficiently large difference in $^{238}U/^{232}Th$ ratio to permit dating of these eruptions. Their results had only a general agreement with K-Ar ages.

Fukuoka and Kigoshi (1974) suggested the use of zircon-glass pairs as the preferable phases for ^{230}Th dating of silicic rocks. They showed that their results were consistent with radiocarbon and fission track ages.

Allegre and Condomines (Allegre, 1968; Allegre and Condomines, 1976, 1982; Condomines, 1978; Condomines and Allegre, 1980; Condomines and others, 1976; Condomines and others, 1981a; Condomines and others, 1981b; and Condomines and others, 1982) have studied U/Th systematics of mafic volcanic rocks from a variety of tectonic environments. Their aim was to apply the systematics developed for Rb/Sr age dating to U/Th dating of young volcanic

rocks. In this way geochemical information on magmatic processes can be obtained in addition to the ages of the rocks. Their work has provided the theoretical background necessary for interpretation of magmatic processes using U/Th systematics.

Theory

Introduction

The theory of radioactive decay and growth has been known for many years. This information is available from many sources, for example Friedlander and others (1981). The following discussions are intended to provide the background necessary for the application of the principles of nuclear physics to studies of ^{230}Th-^{238}U disequilibrium.

Radioactive Decay and Growth

Consider a radioactive decay series of k-1 radionuclides, following the decay path:

$$I_1 \xrightarrow{\lambda_1} I_2 \xrightarrow{\lambda_2} I_3 \xrightarrow{\lambda_3} \ldots I_n \xrightarrow{\lambda_n} \ldots I_k \quad \text{stable},$$

where, λ_n = decay constant of isotope I_n, and the halflife is given by:

$$T_{1/2} = \frac{\ln 2}{\lambda_n} .$$

The change in the number of atoms of I_1 per unit time is given by the fundamental decay equation:

$$\frac{dN_1}{dt} = -\lambda_1 N_1 \quad , \qquad (1)$$

where, N_1 = number of atoms present and $\lambda_1 N_1$ represents the disinteqration rate or <u>activity</u> $(A)^1$ of I_1. The measured count rates are related to the activities by a proportionality constant c, which represents the counting efficiency. Therefore:

$$(A) = c\lambda N \ ;$$

c will be considered to be 1 for the following discussions.

Integration of equation (1) yields the exponential law for the decay of a radioactive species.

$$N_1 = N_1^o \ e^{-\lambda_1 t} \quad , \qquad (2)$$

where N_1^o is the number of atoms present at t = 0.

Now consider the general case where one radioactive species, I_1, decays to a second radioactive species, I_2. The behavior of N_1 is described in equation (1) and the production of N_2 is controlled by the activity of I_1, $\lambda_1 N_1$. N_2 decays at a rate $\lambda_2 N_2$. Therefore:

$$\frac{dN_2}{dt} = \lambda_1 N_1 - \lambda_2 N_2$$

OR

$$\frac{dN_2}{dt} = \lambda_1 N_1^o \ e^{-\lambda 1 t} - \lambda_2 N_2$$

---

[1] Activity is denoted by parentheses.

taking equation (2) into account. Integration of this first order differential equation yields:

$$N_2 = \frac{\lambda 1}{\lambda_2 - \lambda_1} N_1^o \left(e^{-\lambda 1 t} - e^{-\lambda_2 t}\right) + N_2^o \; e^{-\lambda_2 t}$$

OR (3)

$$N_2 = \frac{\lambda 1}{\lambda 2 - \lambda 1} N_1 \left(1 - e^{(\lambda_1 - \lambda_2)t}\right) + N_2^o \; e^{-\lambda_2 t} \quad .$$

In this same way, an expression is obtained for N_3 by integration of the equation:

$$\frac{dN_3}{dt} = \lambda_2 N_2 - \lambda_3 N_3 \quad ,$$

where N_2 is given by equation (3). The process can be carried out for all radioactive isotopes in the series using the general equation:

$$\frac{dN_n}{dt} = \lambda_{n-1} N_{n-1} - \lambda_n N_n \quad .$$

Bateman (1910) developed the solution for a chain of n members assuming that at t = 0 the parent isotope (n = 1) is the only one present:

$$N_n = C_1 e^{\lambda_1 t} + C_2 e^{-\lambda_2 t} + \ldots C_n e^{-\lambda_n t},$$

where:

$$C_1 = \frac{\lambda_1 \lambda_2 \cdots \lambda_{n-1}}{(\lambda_2 - \lambda_1)(\lambda_3 - \lambda_1) \cdots (\lambda_n - \lambda_1)} N_1^o \quad ,$$

$$C_2 = \frac{\lambda_1 \lambda_2 \cdots \lambda_{n-1}}{(\lambda_1 - \lambda_2)(\lambda_3 - \lambda_2) \cdots (\lambda_n - \lambda_2)} N_1^o \quad ,$$

$$C_n = \frac{\lambda_1 \lambda_2 \cdots \lambda_{n-1}}{(\lambda_1 - \lambda_n)(\lambda_2 - \lambda_n) \cdots (\lambda_{n-1} - \lambda_n)} N_1^o \quad .$$

Radioactive Equilibrium and Disequilibrium

Applying equation (3) to radioactive (parent-daughter) pairs, two general cases can be distinguished, depending upon which of the two nuclides has the longer half-life. This study involves the half-lives T_1 and T_2, where $T_1 > T_2$ and therefore $\lambda_1 < \lambda_2$.
In this case, the activities of parent and daughter become constant after a time that is long compared with T_2.

When t is sufficiently long with respect to T_2, $e^{-\lambda_2 t}$ is negligible compared to $e^{-\lambda_1 t}$, and $N_2^o e^{-\lambda_2 t}$ is negligible. Therefore equation 3 becomes:

$$N_2 \simeq \frac{\lambda_1}{\lambda_2 - \lambda_1} N_1^o e^{-\lambda_1 t} ,$$

and since $N_1 = N_1^o e^{-\lambda_1 t}$,

$$N_2 \simeq \frac{\lambda_1}{\lambda_2 - \lambda_1} N_1 .$$

The activities are related by:

$$\lambda_2 N_2 \simeq \frac{\lambda_2}{\lambda_2 - \lambda_1} (\lambda_1 N_1) ,$$

and

$$\frac{\lambda_2 N_2}{\lambda_1 N_1} \simeq \frac{\lambda_2}{\lambda_2 - \lambda_1} \qquad (4)$$

expresses the transient equilibrium that is reached between daughter and parent activities. The limiting case of equilibrium occurs if

$\lambda_1 << \lambda_2$ ($T_1 >> T_2$) and the parent activity does not decrease measurably during many daughter half-lives. Here:

$$\lambda_1 N_1 \approx \lambda_2 N_2.$$

The activities of the two isotopes are equal, and both isotopes decay with the parent half-life, a condition known as secular equilibrium. In this case, equation (3) can be simplified

$$N_2 = \frac{\lambda_1}{\lambda_2} N_1 (1-e^{-\lambda_2 t}) + N_2^o e^{-\lambda_2 t} . \qquad (5)$$

Secular equilibrium is reached in natural radioactive series after several half-lives of the longest lived daughter in the series. After this time, the activities of the isotopes in the series are equal:

$$\lambda_1 N_1 = \lambda_2 N_2 = \ldots = \lambda_n N_n = \ldots = \lambda_{k-1} N_{k-1},$$

and a state of equilibrium exists.

A state of disequilibrium will result any time there is physical or chemical fractionation between two isotopes in the series. Fractionation results in an inequality of the ratios of their activities. Closed-system evolution of a disequilibrium system results in reestablishment of equilibrium.

Natural Radioactive Series

All naturally occurring elements with an atomic number greater than 83 (bismuth) are radioactive. These elements belong to chains involving successive decays, and all of the elements in one such chain constitute a radioactive family or series. There are three of these naturally occurring radioactive series: ^{238}U, ^{232}Th, and ^{235}U (fig. 1). These series include nuclides with differing

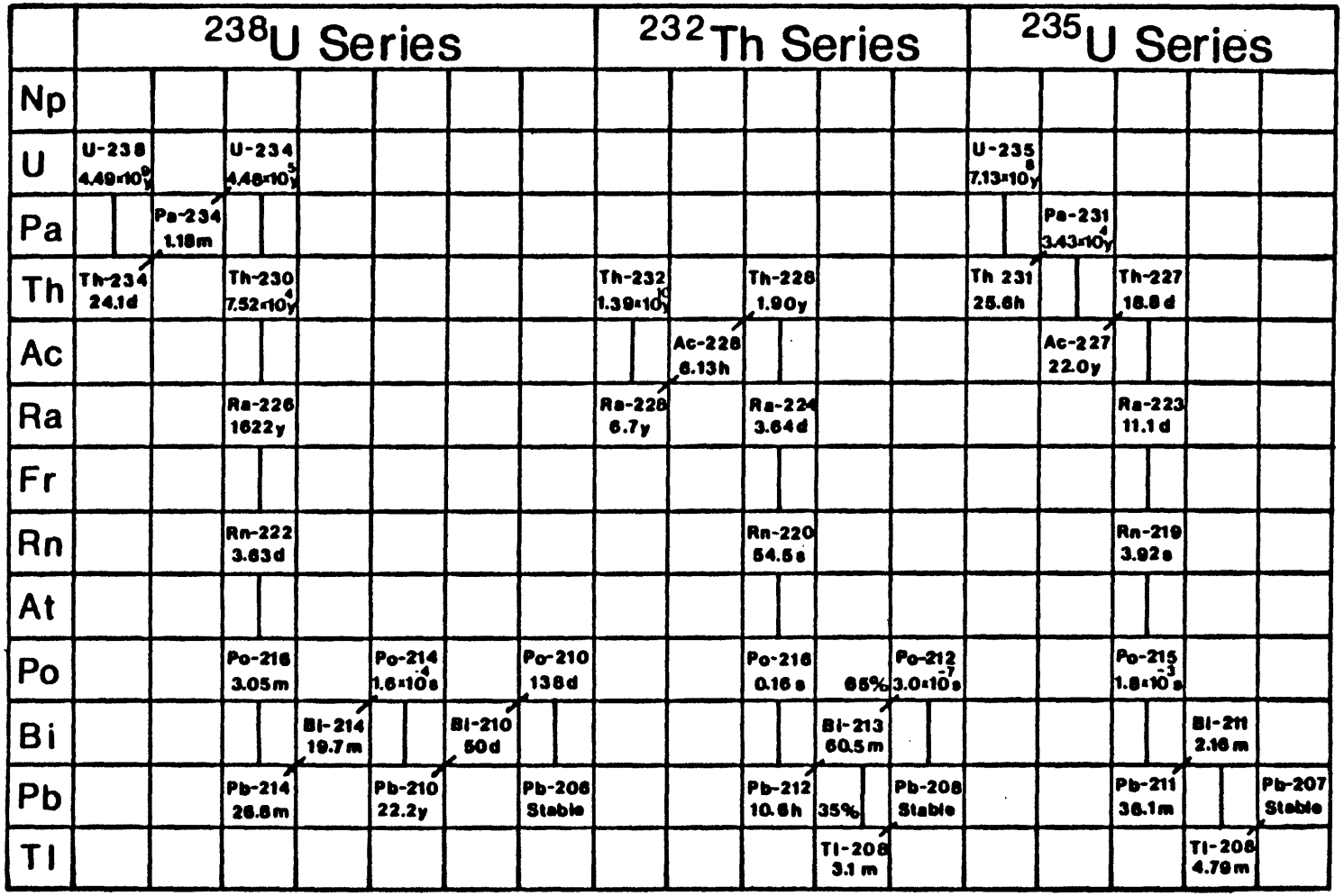

Figure 1. Natural radioactive series (after Ku, 1966), showing half lives and branching ratios.

chemical properties and a wide range of half-lives. Magmatic processes can fractionate uranium and thorium and result in disequilibrium between parents and daughters in the decay series. If the systems remain closed, these separated nuclides will approach a new equilibrium on a time scale dictated by their respective decay constants (λ_n).

^{238}U - ^{230}Th System

The geochronologically important part of tne ^{238}U decay series consists of:

$$^{238}U \longrightarrow {}^{234}Th \longrightarrow {}^{234}Pa \longrightarrow {}^{234}U \longrightarrow {}^{230}Th \longrightarrow .$$

^{230}Th, a nuclide in the ^{238}U series, has a half-life of 75,200 years. ^{238}U has a half-life of 4.49×10^9 years and is separated from the ^{230}Th by three isotopes (fig. 1): ^{234}Th, ^{234}Pa, and ^{234}U. The first two isotopes have short half-lives and therefore rapidly come to equilibrium with ^{238}U. ^{234}U has a half-life of 4.48×10^5 years and is expected to be in equilibrium with ^{238}U because these two uranium isotopes will not be fractionated by magmatic processes. When these four isotopes are in equilibrium, ^{230}Th can be considered a direct product of ^{238}U, since:

$$(^{238}U \cdot \lambda_{238}) = (^{234}U \cdot \lambda_{234}).$$

For any mineral phase crystallized from the magma at t=0, tne ^{230}Th content at time t is given by:

$$\left(^{230}Th\right)_t = \left(^{238}U\right)_t (1 - e^{-\lambda_{230} t}) + \left(^{230}Th\right)_o e^{-\lambda_{230} t}, \quad (6)$$

where the first term is the growth of ^{230}Th since crystallization and the second term is the remaining initial ^{230}Th.

Assume:

$$\left(\frac{^{234}U}{^{238}U}\right) = \left(\frac{^{234}U}{^{238}U}\right)_o = 1.0$$

and

$$\left(\frac{^{238}U}{^{232}Th}\right) = \left(\frac{^{238}U}{^{232}Th}\right)_o$$

(due to their long half-lives, 4.49×10^9 and 1.39×10^{10} years respectively). Further assume that $\left(\frac{^{230}Th}{^{232}Th}\right)_o$ is the same for all phases crystallized from the magma at time t, and that $(^{232}Th)_t \simeq (^{232}Th)_o$ (due to its long half-life). Equation (6) can then be written:

$$\left(\frac{^{230}Th}{^{232}Th}\right)_t = \left(\frac{^{238}U}{^{232}Th}\right)_t (1-e^{-\lambda t}) + \left(\frac{^{230}Th}{^{232}Th}\right)_o e^{-\lambda t} \quad . \qquad (7)$$

All mineral phases crystallized from a magma at the same time are expected to satisfy this relation. The $(^{230}Th/^{232}Th)$ ratios of mineral phases plotted versus their $(^{238}U/^{232}Th)$ ratios will lie on a straight line (isochron) with a slope of:

$$1 - e^{-\lambda t} ,$$

and a y intercept of:

$$\left(\frac{^{230}Th}{^{232}Th}\right)_o e^{-\lambda t} .$$

At t=0 each mineral phase has the same inital $\left(\frac{^{230}Th}{^{232}Th}\right)_o$ ratio but a

different $\left(\frac{^{238}U}{^{232}Th}\right)$ ratio due to chemical and physical fractionation processes. When plotted on the isochron diagram these points fall on a straight horizontal line with an ordinate equal to $\left(\frac{^{230}Th}{^{232}Th}\right)_o$.

When $t >> 7.52 \times 10^4$, $(^{230}Th) = (^{238}U)$, representing radioactive equilibrium. All points lie on a straight line, with a slope of 1 (equiline), that passes through the origin. The isochron rotates around a fixed point defined by the intersection of the isochron with the equiline (fig. 2). The measured slope and y intercept of the isochron can then be used to solve for the time of crystallization of the rock and the initial $(^{230}Th/^{232}Th)$ ratio of the magma, which is the ordinate of the intersection of the isochron and the equiline.

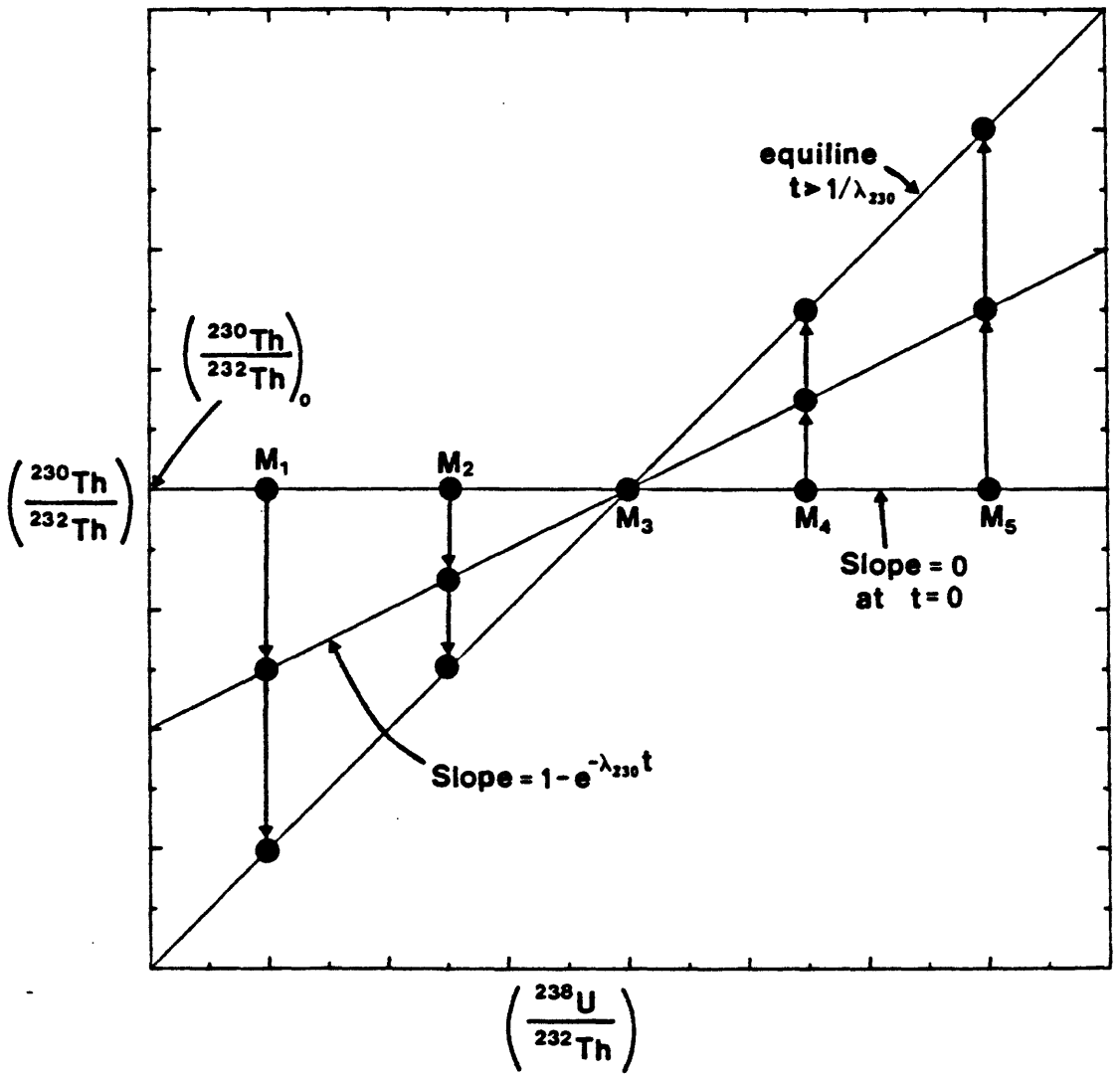

Figure 2. Generalized isochron diagram, Equiline represents radioactive equilibrium. M_1 - M_5 follow vertical trajectories toward the equiline.

ANALYTICAL PROCEDURES

Mineral Separates

Each mineral phase analysed requires a minimum of 10 g of material with a purity approaching 100 percent. Mineral separates were prepared following the procdures described by Allman and Lawrence (1972) and Hutchison (1974). Samples were first cleaned of all weathered surfaces and broken into managable sizes. Coarse crusning was performed in a standard chipmunk jaw crusher. Mafic inclusions were then picked from the crushed rock material. Fine crushing was done using a standard roller mill. Fine material was removed from the sample periodically by sieving using a Rotap sieve shaker. The final crushed sample was sized using 0.59 mm, 138 μm, 98 μm, 59 μm, 49 μm, 41 μm, and 29 μm sieves.

Each size fraction was examined under a binocular microscope to determine the most suitable fraction for subsequent procdures. The size fractions used were those that had a majority of monomineralic grains. Nonmagnetic phases were concentrated from the selected fractions using a Carpco electromagnetic separator. A good glass-plagioclase concentrate requiring only one heavy liquid separation could usually be obtained.

The samples were washed to remove dust before performing heavy liquid separations using bromoform, methylene iodide, and neothene.

The first separation divided the sample into two groups: a light fraction of quartz, plagioclase, and glass, and a heavy fraction of mafic minerals (magnetite, hornblende, biotite, and pyroxene). Plagioclase was separated from the light fraction by a second heavy liquid separation and then cleaned using a Frantz isodynamic magnetic separator. Quartz and glass were not normally used. Magnetite was separated from other mafic minerals with a hand magnet. Magnetite samples were ground carefully with a 100 percent alumina mortar and pestle to dislodge clinging groundmass and glass. A 99 percent pure magnetite separate was obtained by alternating hand magnet separations and grinding. Hornblende, biotite and pyroxene were separated by a series of heavy liquid separations. Biotite was further purified using a ball mill and a mica table. Clinging groundmass was removed from hornblende and pyroxene by ultrasonic cleaning.

Reagents and Apparatus

Tracers

The tracer used in the U/Th isotopic analysis was an acid solution of ^{232}U (25.16 dpm/ml) and its daughter product ^{228}Th (24.6 dpm/ml). They were made available by Dr. J. N. Rosholt, U. S. Geological Survey, Denver. The spike initially consisted of purified ^{232}U and the ^{228}Th has subsequently grown in. In transient equilibrium, the ($^{228}Th/^{232}U$) activity ratio equals

1.0267. At the start of this study, the activity ratio of the spike was 0.9922.

The production of ^{228}Th from ^{232}U can be described by the equation:

$$N_2 = \frac{\lambda_1}{\lambda_2-\lambda_1} \quad N_1^o(e^{-\lambda_1 t} - e^{-\lambda_2 t}) + N_2^o\, e^{-\lambda_2 t} \ ,$$

where: N_1^o = parent at t = 0 and N_2^o = daughter at t = 0.

At t = 0 there is no daughter, therefore:

$$N_2^o\, e^{-\lambda_2 t} = 0.$$

The decay of ^{232}U is described by the equation:

$$N_1 = N_1^o e^{-\lambda_1 t} \ .$$

By combining the two equations, an equation for the activity ratio is obtained:

$$\left(\frac{^{228}Th}{^{232}U}\right) = \frac{\lambda_2\, N_2}{\lambda_1\, N_1} = \frac{\lambda_1\lambda_2}{(\lambda_2-\lambda_1)\lambda_1} \quad (1-e^{-(\lambda_2-\lambda_1)t})$$

$$= \frac{\lambda_2}{\lambda_2-\lambda_1} \quad (1-e^{-(\lambda_2-\lambda_1)t}) \ .$$

The activity ratio for the spike used in this study is described by the equation:

$$\left(\frac{^{228}Th}{^{232}U}\right) = 1.0267 \left[1 - e^{(-9.6623 \times 10^{-4})(3036.2 + Ts)}\right] \ ,$$

where: $\frac{\lambda_2}{\lambda_2-\lambda_1} = 1.0267$,

$\lambda_2 - \lambda_1 = 9.6623 \times 10^{-4}$,

Ts = date (Julian) that the thorium and uranium samples were separated,

3063.2 = time (in days) since ^{232}U spike was purified.

Carriers

Uranium has two stable oxidation states (IV and VI) in aqueous solutions. Uranium must be maintained in the oxidized (VI) state during separation procedures as U(IV) behaves much like thorium, and the two U species may be separated (Goldberg and Koide, 1958). Uranium (VI) is the stable species in the presence of oxygen and ferric iron (Thurber, 1963). Hydroxide precipitation procedures may affect the iron oxidation state when the working solution is warm; therefore hydroxide precipitations should be performed only on solutions at room temperature. If, during a hydroxide precipitation, the solution turns green, at least some of the iron has been reduced. The uranium may also have been reduced; the sample should be oxidized by stirring in the presence of air before proceeding with the separation.

Carriers are used to insure quantitative precipitation of uranium and thorium during chemical procedures. Most of the samples analyzed contained sufficent quantities of the naturally occurring carrier elements, iron, aluminum, and zirconium. Fe(III) carrier was added for analyses of plagioclase and glass and in the thorium purification procedure.

Reagents and Chemical Apparatus

Except in the following cases analytical grade reagents are sufficiently pure to permit use without further purification. A saturated solution of $Al(NO_3)_3$ was prepared by saturating 4N HNO_3 with $Al(NO_3)_3$. The saturated solution was purified using ethyl acetate to remove any uranium or thorium.

The Fe(III) carrier was prepared by dissolving 65.8 g of $FeCl_3 \cdot nH_2O$ in 100 ml of 8N HCl. The Fe(III) carrier was purified by extraction into isopropyl ether, followed by back extraction into 1N HCl.

TTA solution (0.4N) was made by dissolving 2.218 g of 4-4-4 trifluro-1-(2-thienyl)-1, 3-butanedione (TTA) in 25 ml benzene. To eliminate oxidation problems, the TTA solution was prepared in 25 ml batches and stored for no more than one month.

To eliminate potential contamination between samples, ion exchange resins were used once and discarded. Because the ion exchange resin breaks down when left in the nitrate form, whenever the uranium and thorium separation procedure was carried out over a two day period, the ion exchange column was left in the chloride form.

Teflon, glass, and plastic labware were washed in CMS 1·2·2 cleaning compound (phosphate-free), and teflon and glass labware were soaked for 12-16 hours in concentrated HNO_3. Distilled water was used to rinse all labware and to prepare all reagents.

Chemistry

Introduction

Procedures for the separation of uranium from thorium suitable for use on rock materials could not be found in the literature. Accordingly, the early stages of this investigation involved modifying procedures described in the literature for other materials. Uranium and thorium separation techniques developed for deep sea sediments by Ku (1966) were modified for this study by applying analytical chemical data compiled by the U. S. Atomic Energy Commission (Hyde, 1960; Gindler, 1962). The objective was to develop procedures as simple as possible that produced yields sufficient to obtain acceptable counting statistics. The yields obtained ranged between 15 and 75 percent for uranium and between 15 and 90 percent for thorium. The procedures used are detailed here to facilitate use by subsequent workers. Potential problems are noted and countermeasures given. A chemistry flow chart is given in Appendix 1.

Dissolution of Rock Samples

The dissolution procedure used in this study was designed to dissolve the sample totally. This insures that radionuclides of interest are completely released into an aqueous phase with Cl^- as the major anion, facilitating subsequent procedures. The dissolution procedure used was as follows. Weigh out a sufficient quanity of mineral separate to obtain approximately 10 µg of

uranium. Place the sample in a 400 ml teflon beaker and add an aliquot of spike. Ideally the activity of the spike should approximate the activity of the sample. For samples low in iron (i.e. plagioclase) add 0.5 ml of Fe(III) carrier. Add 5 ml each of concentrated acid per gram of sample in the following order: HNO_3, $HClO_4$, and HF. Cover the beaker with a teflon watch glass and place on a hot plate with a surface temperature of approximately 100°C. After 12 to 18 hours uncover the beaker and volatilize the acids by increasing the surface temperature of the hot plate to 225-250°C. For large samples it may be preferable to use half the acid and repeat the procedure. After fuming ceases, remove the beaker from the hot plate and cool to room temperature. Add an additional 2 ml each of concentrated HNO_3, $HClO_4$, and HF per gram of sample. Return the sample to the hot plate (surface temperature 225-250°C) until fuming ceases. Remove the sample from the hot plate and cool to room temperature.

Dissolve the decomposed sample in 6N HCl. Heating the sample at a low temperature facilitates dissolution. Place the sample in teflon centrifuge tubes and centifuge at high rpm. If a residue remains, HNO_3 or aqua regia will usually dissolve it. If some residue still remains, repeat the second acid treatment with 5 ml each of concentrated HNO_3, $HClO_4$, and HF.

Preliminary Treatment of Sample Solution

Transfer the dissolved sample to a 1000 ml plastic beaker and dilute with distilled water to approximately 600 ml. Add

concentrated NH_4OH to the solution until a pH of 7-8 is reached. Uranium and thorium co-precipitate with $Fe(OH)_3$, $Al(OH)_3$, and other hydroxides. Let the precipitate settle, decant, and discard the supernate. Wash the precipitate twice by adding distilled water, shaking, centrifuging, decanting, and discarding the liquid.

Many samples require removal of iron and/or aluminum at this time. Iron is removed by dissolving the precipitate in enough concentrated HCl to make an 8N solution. Place the dissolved sample in a separatory funnel and add an equal volume of isopropyl ether. Shake thoroughly and release excess pressure occasionally. Repeat the isopropyl ether extraction, adding enough concentrated HCl to maintain an 8N solution, until the orange-yellow color of the solution changes to light yellow. If the isopropyl ether separates into layers, the solution is too acidic; adjust by adding distilled water. Collect the aqueous phase in a glass beaker, and gently heat on a hot plate to volatilize any remaining ether. Remove the sample from the hot plate and cool to room temperature. Dilute and reprecipitate the sample with concentrated NH_4OH. Centrifuge the precipitate and discard the supernate. Wash the precipitate with distilled water at least twice. If the volume of precipitate is large and the precipitate is tan in color, an aluminum extraction is necessary. Wash the precipitate with hot 3N NaOH to remove the aluminum, centrifuge and decant, discarding the NaOH solution. Repeat the NaOH wash if a large amount of precipitate remains. Wash the remaining precipitate with distilled water two or three times to remove remaining NaOH. Plagioclase and silicic whole-rock samples

require only an aluminum extraction; magnetite requires only an iron extraction; hornblende, biotite, and pyroxene may require both extractions.

Separation of Uranium and Thorium

Uranium and thorium are separated using anion exchange resins in columns. The sample is first run through the column with resin treated with 8N HCl. In this form, the resin retains uranium and Fe(III) and passes thorium and aluminum. The sample is then run through resin treated with 8N HNO_3 to separate thorium.

Prepare an anion exchange column using Bio Rad AG 1-X8 (chloride form), 100-200 mesh anion resin. Wash the resin twice with distilled water and twice with 8N HCl. Place a glass wool plug in the end of a glass column (approximately 1 cm X 10 cm with a 50 ml reservoir) and put treated resin in the column to a height of 9 to 9.5 cm. Wash the column with 3 to 4 column volumes of 8N HCl.

Dissolve the precipitate in enough concentrated HCl to obtain an 8N HCl solution. In some samples, a white titanium precipitate forms; centrifuge and discard the precipitate. Put the cooled solution into the reservoir of the prepared anion exchange column. The solution that passes through the column contains the thorium and is collected in a 100 ml glass beaker. When all the sample solution nas passed through the column, pass an additional 20 ml of 8N HCl through the column. Collect the wash in the thorium beaker and set aside.

The reddish-orange band on the anion exchange column contains uranium and iron (the band is not always easily visible). Elute the uranium and iron with 0.1N HCl, collecting the solution in a 100 ml glass beaker. The uranium fraction is eluted when the HCl passing through the column is clear. Pass an additional two column volumes of 0.1N HCl through the column and collect in the uranium beaker. Evaporate the solution to dryness on a hot plate.

Place the solution containing thorium in a 400 ml plastic beaker and dilute to approximately 250 ml. Rinse the beaker that contained the solution, and add the rinse to the sample. Add 0.2 ml of Fe(III) carrier to the thorium fraction. Put a teflon stir bar in the beaker and place it on a magnetic stirrer. Stir the sample for approximately 15 minutes. Add concentrated NH_4OH to precipitate the iron, aluminum, and thorium. Centrifuge the sample and discard the supernate. Wash the precipitate with distilled water at least twice. If a large volume of precipitate remains, it is probably aluminum, and an aluminum extraction should be done. Add enough concentrated HNO_3 to make an 8N solution (err on the weak side; too concentrated an acid will cause the column to gel and may result in loss of the sample).

Convert the same anion exchange resin used for the initial separation of the uranium and thorium to a nitrate form. Pass several column volumes of 8N HNO_3 through the anion exchange column (minimum of 40 ml). When the resin is converted, pass the cooled thorium fraction through the column. Once the solution has passed through the column, pass an additional two column volumes of

8N HNO_3 through the column and discard the solution. Elute the thorium from the resin with 40 ml of 8N HCl and collect the solution in a 50 ml glass beaker. Place the beaker on a hot plate and take to dryness. The beaker should have little or no residue remaining. A brownish residue is probably iron. Dissolve the sample in 8N HCl, perform an iron extraction, and take the sample to dryness.

Magnetite separates may have large amounts of the transition metals cobalt and copper. Cobalt colors the anion resin green, and copper colors the anion resin brown, but they do not appear to affect the separation of uranium and thorium.

Uranium Purification

Take up the residue in 10 to 15 ml of 8N HCl and transfer to a 30 ml separatory funnel. Wash the beaker with 8N HCl and add the wash to the solution in the separatory funnel. Add a volume of isopropyl ether equal to the volume of sample solution. Add a few drops of concentrated HCl and shake the separatory funnel. Separate the aqueous phase. Repeat until the aqueous phase is colorless. Transfer the aqueous phase to a glass beaker and take to dryness on a hot plate. Repeat the isopropyl ether extraction if a dirty-looking, brownish residue is present. If a residue still remains, it is probably organic residue from the isopropyl ether. To remove it, add 3 to 5 ml of concentrated HNO_3 and take to dryness on a hot plate.

Take up the uranium fraction in 3 to 4 ml of 4N HNO_3 saturated with $Al(NO_3)_3$. Place the beaker on the hot plate and heat the

solution to approximately 100°C. With a teflon policeman, scrape the bottom of the beaker to insure that all of the uranium is dissolved. Transfer solution to a 15 ml glass centrifuge tube. Rinse the beaker with 1 ml of the $Al(NO_3)_3$ solution and add it to the centrifuge tube. Cool the solution to room temperature. Add 2 to 3 ml of ethyl acetate and emulsify for 4 to 5 minutes. If crystals form, remove the ethyl acetate and reheat the $Al(NO_3)_3$ solution. Centrifuge the mixture, pipet off the ethyl acetate, being careful not to take up any of the $Al(NO_3)_3$ solution, and place it in a clean glass centrifuge tube. Repeat the ethyl acetate extraction twice more. The uranium is now in the ethyl acetate. Back extract the uranium by adding an equal volume of distilled water. Emulsify 4 to 5 minutes, centrifuge, and remove the water (lower portion). Place the water containing uranium in a clean 50 ml glass beaker. Repeat the back extraction twice more. Place the beaker containing the solution on a hot plate and take to dryness. The beaker should have little or no visible residue. If a residue is present, dissolve it in concentrated HNO_3 and take to dryness.

When the solution has evaporated, remove the beaker from the hot plate and cool to room temperature. Take up the sample in 3 to 4 ml of 0.1N HNO_3 (pH = 1), using a teflon policeman to scrape the bottom of the beaker. Transfer the sample to a 15 ml glass centrifuge tube. Rinse the beaker with an additional 2 ml of 0.1N HNO_3 and add it to the centrifuge tube. To remove any thorium from the uranium sample, perform a preliminary TTA extraction. Add 10-15 drops of TTA to the centrifuge tube. Emulsify the sample

several times, then centrifuge. Draw off the TTA with a pipet and discard, being careful not to take up any of the aqueous phase. To extract uranium from the solution, adjust to pH 3 using 1N NaOH, continuing to pH 3.5 using 0.1N NaOH. Repeat the TTA extraction on the pH-adjusted solution three times. Uranium yields are increased if the solution is emulsified every 3 or 4 minutes for 15 minutes between TTA extractions. After each extraction slowly drop the uranium-containing TTA onto a clean, warm stainless steel planchet. When all the benzene has evaporated, heat the planchet to red heat for a few seconds in a bunsen flame to oxidize any remaining organics. The sample is now ready to be placed in the uranium alpha spectrometer.

Thorium Purification

Take up the thorium in 3 to 4 ml of 0.1N HNO_3 (pH = 1). Scrape the bottom of the beaker with a teflon policeman and transfer the solution to a 15 ml glass centrifuge tube. Rinse the beaker with an additional 2 ml of 0.1N HNO_3 and add to the centrifuge tube. Add 10 to 15 drops of TTA to the centrifuge tube, emulsify the sample several times and then centrifuge the sample. Draw off the TTA, being careful not to take up any of the aqueous phase in the pipet. Slowly drop the TTA onto a clean, warm stainless steel planchet. Repeat the TTA extraction twice more. Thorium yields are increased if the solution is emulsified every 3 or 4 minutes for 15 minutes between TTA extractions. When the benzene has evaporated, flame the planchet in the same manner as the uranium sample.

Counting Techniques

Alpha Spectrometry

Four Ortec 576 dual alpha spectrometers with three Davidson 404A routers and a Davidson 4106 pulse height analyzer were used for uranium and thorium isotope analyses. Each alpha spectrometer has two independent channels, each with a 512 keV range. The alpha spectrometers utilize surface barrier type detectors with a 600 mm^2 depletion layer, 100 μm thick. The range of the detectors was modified in order to observe the energies of interest, 3.67 to 6.25 MeV. Peak locations were determined by counting a sample with high counting rate for each isotope (table 1). The counting efficiency of each detector was measured using a standard of known count rate, and the results are listed in table 2.

The signal of the detector varies linearly with the alpha particle energy, if the particle's energy is completely expended in the detector depletion layer. For alpha particles, a depletion layer of 60 μm is necessary to totally absorb the particle energy (Thurber, 1963). The height of the pulse produced is proportional to the energy expended in the detector. The pulses are amplified and then routed to the pulse height analyzer, which records the number of pulses occuring in each energy interval (about 1 keV).

TABLE 1

PEAK LOCATIONS

Counter	Window and Peak Location						
	^{232}U	^{234}U	^{238}U	^{228}Th	^{230}Th	^{232}Th	^{224}Ra
1	313-386 375	203-276 267	84-157 149				
2				52-125 117	192-265 254	343-415 405	416-468 458
3	317-390 382	209-281 274	92-165 156				
4				57-130 117	197-269 260	348-420 409	421-472 462
5	333-405 395	221-294 285	106-179 169				
6				76-149 141	215-288 273	366-439 426	440-491 480
7	344-417 408	229-301 294	112-185 176				
8				67-140 127	203-276 264	358-431 414	432-485 469

TABLE 2

COUNTER EFFICIENCY

Counter	Efficiency
1	0.330
2	0.326
3	0.337
4	0.326
5	0.332
6	0.337
7	0.324
8	0.329

Thin Source Preparation

For uranium and thorium analyses, a thin source is required to reduce uncertainties introduced by interference on the low energy side of the peaks. Thick sources cause broadening of peaks and may cause interference between peak tails on their low energy side (figs. 3 and 4).

Electroplating of samples to obtain a thin source was attempted with less than satifactory results. As a result, the chelating agent TTA was used (Thurber, 1963). TTA extractions are pH dependent (fig. 5) making it possible to use them in the final purification of the sample. Th is extracted at pH = 1, and uranium is extracted at pH = 3.5.

Peak widths (FWHM) were measured on all samples, were satisfactory, and ranged from 50 to 105 KeV. The metal-TTA chelates do not produce a homogeneous source like electroplating. Instead, concentric rings of metal-TTA form when the benzene evaporates. For the amount of material used, the results were satifactory, and the alpha spectra are comparable to those reported by Ku (1966), although slightly broader peaks are to be expected due to the larger areas of our dectectors (600 mm^2 versus 400 mm^2).

Calculations

Peak Corrections

Alpha spectral data were analyzed to determine 100 percent count rates, yields, uranium and thorium concentrations, and relative

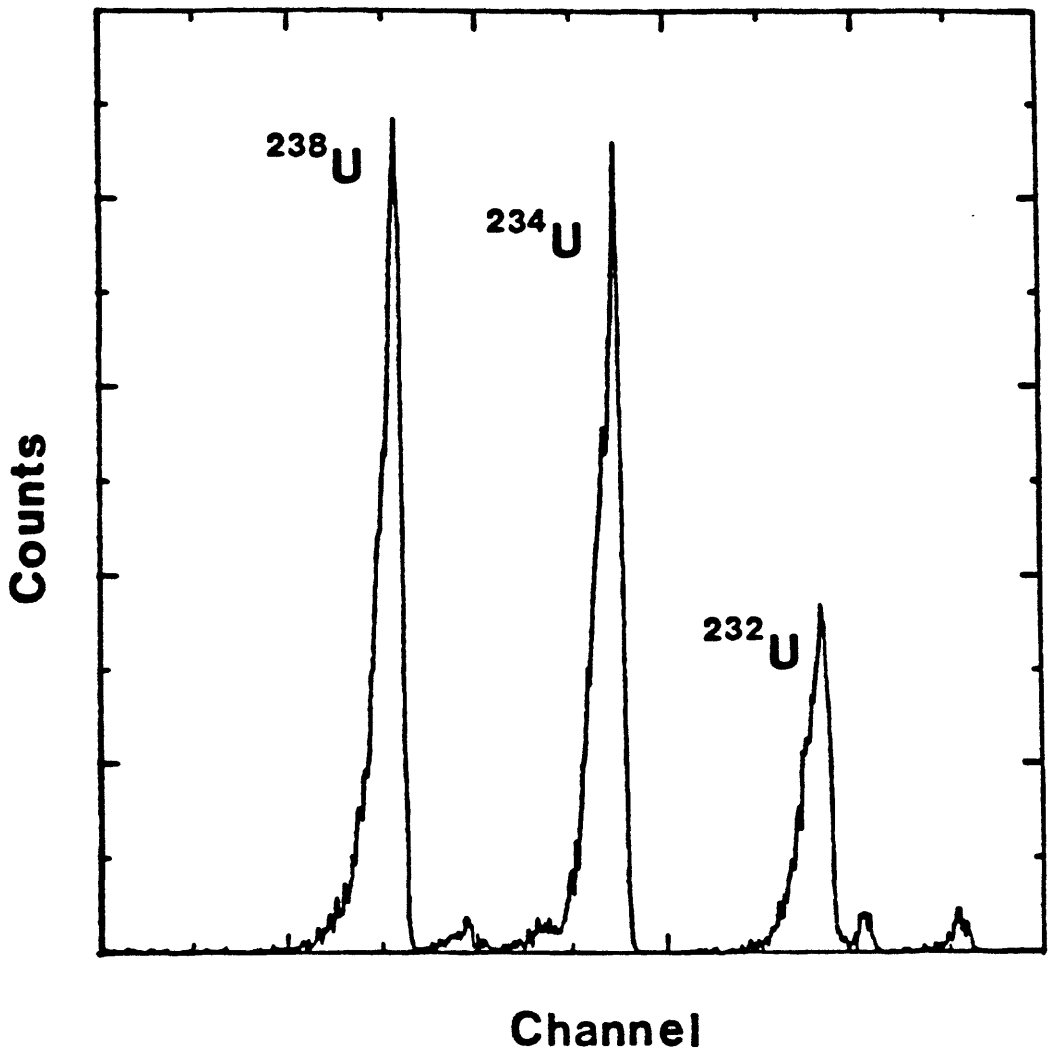

Figure 3. Typical uranium spectrum.

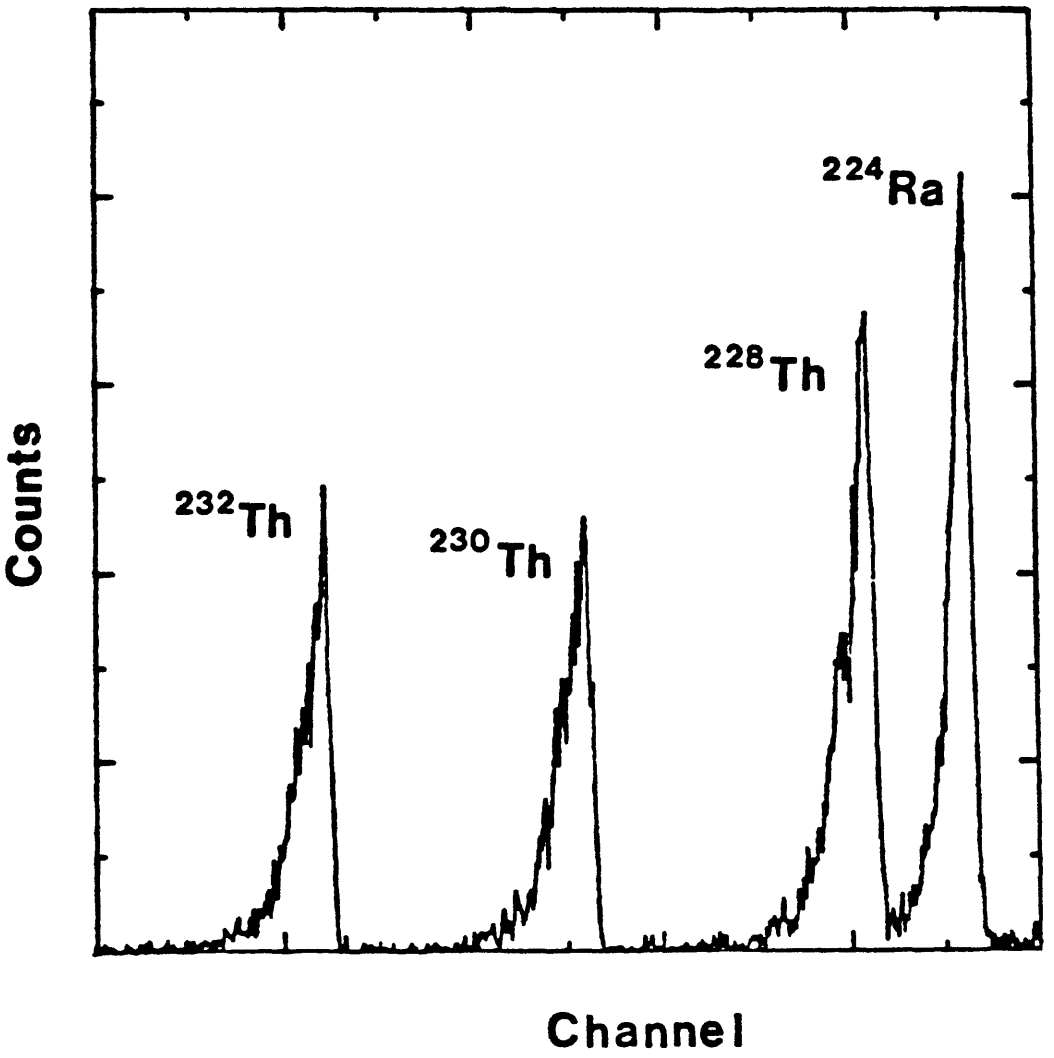

Figure 4. Typical thorium spectrum.

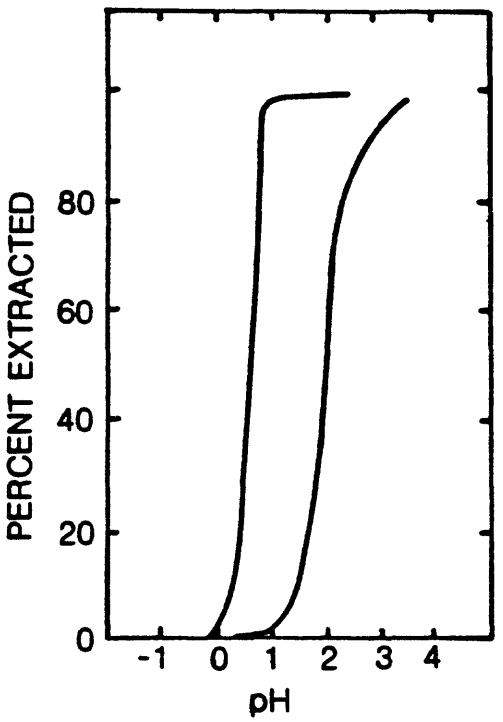

Figure 5. The effect of pH on TTA-benzene extraction of uranium (VI) and thorium (modified from Gindler, 1962).

errors (σ). Corrections were made on the raw data to compensate for background noise, tail effect, and peak interference.

The number of counts under each peak was measured in a 74-channel window, with the exception of the ^{224}Ra peak which was measured using a 53-channel window, because its tail extends beneath the ^{228}Th peak. ^{228}Th was measured twice, once with each window width. The ratio of the two measurements was used to make corrections to the ^{228}Th data.

A peak interference correction is necessary on the ^{232}U data when samples are counted for more than 10,000 minutes. The decay of the ^{232}U spike embeds ^{228}Th in the uranium detectors,

$$^{232}U \xrightarrow[73.6y]{\alpha} {}^{228}Th \xrightarrow[1.93y]{\alpha} {}^{224}Ra \xrightarrow[3.64d]{\alpha} .$$

As a result, ^{228}Th and ^{224}Ra peaks grow <u>in situ</u> and may interfere with the ^{232}U peak (table 3). It is reasonable to assume equilibrium between ^{228}Th and ^{224}Ra, due to their short half-lives. It is therefore possible to calculate a corrected ^{232}U value,

$$(^{228}Th) \approx (^{224}Ra).$$

Therefore:

$$(^{232}U_c) = (^{232}U) + (^{228}Th) - (^{224}Ra),$$

where $(^{232}U_c)$ is the corected value.

To avoid systematic errors caused by <u>in situ</u> decay, the same four detectors were always used to analyze uranium.

TABLE 3

PEAK INTENSITIES
[Modified after Weast, 1979]

Isotope	Energy (MeV)	Particle Intensity
Uranium		
232	5.32	68.6
	5.263	31.2
	5.137	0.28
234	4.773	72
	4.722	28
	4.599	0.35
235	4.597	4.6
236	4.493	74
238	4.195	77
	4.147	23
	4.135	0.23
Thorium		
228	5.424	71
	5.342	28
	5.211	0.4
	5.176	0.2
230	4.684	76
	4.617	24
	4.474	0.12
232	3.994	77
	3.935	23
	3.809	0.2
Radium		
224	5.684	94.5
	5.447	5.5

The raw data are converted to count rates (C) and corrected for background noise, B (table 4):

$$C = \frac{N}{T} - B \ ,$$

where: N = number of counts in window,

T = time counted in minutes.

Subsequent corrections are performed on the count rates.

^{228}Th data are corrected for the tail interference of the ^{224}Ra peak, contribution from the 5.342 MeV peak of ^{224}Ra, in situ decay of ^{232}Th to ^{228}Th, and decay of ^{228}Th to ^{224}Ra. The ^{224}Ra peak tail contributes to tne total number of ^{228}Th counts. Using the assumption that both peaks have the same shape, it is possible to correct for the tail interference of ^{224}Ra

$$(^{224}Ra)\left(\frac{^{228}Th_o}{^{228}Th_n}\right) - (\ ^{224}Ra) \ ,$$

where: $^{228}Th_o$ = uncorrected ^{228}Th count rate,

$^{228}Th_n$ = ^{228}Th count rate calculated for the 53 channel reading.

The contribution of the ^{224}Ra peak located under the ^{228}Th peak is calculated in a similar manner. The major ^{224}Ra peak (5.68 MeV) represents 94.5 percent of ^{224}Ra activity; the peak under the ^{228}Th peak (5.45 MeV) represents 5.5 percent of the ^{224}Ra activity. Therefore the smaller ^{224}Ra peak contributes:

$$\left(\frac{5.5}{94.5}\right) ^{224}Ra \left(\frac{^{228}Th_o}{^{228}Th_n}\right)$$

to the ^{228}Th count rate. ^{232}Th and ^{228}Th are in secular

TABLE 4

BACKGROUND

Counter	Background (cpm) High Channels	Low Channels
1	0.019	0.023
2	0.0195	0.017
3	0.018	0.012
4	0.0215	0.0165
5	0.0175	0.0185
6	0.011	0.0075
7	0.014	0.0065
8	0.014	0.008

equilibrium ($\lambda_{232} << \lambda_{228}$). Therefore the activity (count rate)of the ^{232}Th is equal to the activity of the ^{228}Th that has grown in situ from the decay of ^{232}Th in the sample. The correction is made by subtraction of the (^{232}Th) from ($^{228}Th_o$). The ^{224}Ra starts to grow in situ from the time the thorium is plated on the planchet. To determine the absolute count rate, it is necessary to compensate for the decay of ^{228}Th by multiplying the corrected ^{228}Th peak values by $e^{\lambda_{228}t}$, where λ_{228} equals the decay constant of ^{228}Th, and t equals the delay between time of separation and time counted.

The equation for all corrections made to the (^{228}Th) is:

$$^{228}Th = (^{228}Th_o) - (^{224}Ra)(F-1) - 0.582(F)(^{224}Ra) - (^{232}Th)\ e^{\lambda 228t},$$

where: $F = \left(\frac{^{228}Th_o}{^{228}Th_n}\right)$.

Yield Calculation

Yields are determined in order to calculate 100 percent count rates:

$$C_{100\%} = \frac{C}{Y},$$

where: C = measured count rate,

Y = yield.

The yields are calculated using the spike ratio data (^{232}U and ^{228}Th). The data are corrected for decay of ^{232}U, disequilibrium in the spike ratio, and for detector efficiency, in order to obtain absolute activity.

$$Y_{Th} = \frac{^{228}Th}{(7.55)(V_s)(S_r)e^{-\lambda 232 t}}$$

and

$$Y_U = \frac{^{232}U}{(7.55)(V_s)e^{-\lambda 232 t}} ,$$

where: 7.55 = 30 percent (detector efficiency) of 25.16 dpm/ml (^{232}U activity),

V_s = spike volume,

S_r = spike ratio,

t = time since calibration of the spike.

Uranium and Thorium Concentration

U and Th concentration calculations were made for whole-rock studies. ^{238}U and ^{232}Th count rates were used, as they are the dominant naturally occurring species (99.27 percent and 100 percent respectively):

$$U_{ppm} = \frac{(^{238}U)}{(.746)(wt)(E)} ,$$

$$Th_{ppm} = \frac{(^{232}Th)}{(.246)(wt)(E)} ,$$

where: specific activity of 1 µg ^{238}U = 0.746 dpm,

specific activity of 1 µg ^{232}Th = 0.246 dpm (Hyde and others, 1971),

wt = sample weight,

E = detector efficiency.

Errors

A standard of known concentration was used to calculate detector efficiency. Efficiencies ranged between 0.324 and 0.337 with a calculated error of 1 percent or less. The counter efficiency can vary due to the variation in the distribution of sample on the surface of the stainless steel planchet. To eliminate variation in the counter efficiency care should be taken to insure that the sample is distributed evenly over the surface of the planchet and that the planchet is centered in the detector. The error has a greater affects on the yield and concentration calculations, with little or no effect on calculations of isotopic ratios.

Possible sources of random error include: 1) contamination of sample material during crushing; 2) contamination from chemical reagents and labware; 3) variation in the detector background; 4) fractionation of spike relative to sample; and 5) statistical counting errors.

To avoid contamination of sample material, care was taken in cleaning all crushing equipment and by working on only one sample at a time. Chemical reagents were checked for contamination periodically with blank runs. Background measurements also were made periodically. To avoid potential fractionation between spike and sample, mechanical loss of the spike-sample mixture was strictly avoided.

Errors due to counting statistics are the only errors that can be quantified on theoretical grounds. If N counts are accumulated in a counting period t, then the standard deviation of N is:

$$\sigma_n = \sqrt{N} \ ,$$

in terms of count rate (S=N/t):

$$\sigma_S = \frac{\sqrt{N}}{t} = \sqrt{\frac{S}{t}} .$$

Standard deviation (σ) of the count rate of, provided that the time counted is short relative to the half-life of the radioactive isotope is:

$$\sigma = \left[\left(\frac{N}{t}\right)^2 + B^2\right]^{\frac{1}{2}} \quad \text{OR} \quad \sigma = \left[\left(\frac{S}{t}\right)^2 + \left(\frac{B^2}{t}\right)\right]^{\frac{1}{2}} ,$$

where: t = time counted,

B = background count rate.

The relative error for count rates in the presence of background count rate (B) is:

$$S_{net} = S - B, \qquad \sigma_{net} = \left[\left(\frac{S}{t}\right) + \sigma_B^2\right]^{\frac{1}{2}} ,$$

where: S = count rate.

The precision of derived quantities $y = F(x,y)$ (e.g. $^{230}Th/^{232}Th$), was computed using the general equation (Crow and others, 1960):

$$\delta y = \left(\frac{\delta F^2}{\delta x}\right)\sigma_x^2 + \left(\frac{\delta F^2}{\delta y}\right)\sigma_y^2 ,$$

where, σ_x and σ_y are the standard deviation of x and y respectively.

Isochron Calculation

Isochrons and their errors were calculated using the least squares cubic method of York (1967; 1969) and solving for the slope, b:

$$b^3 \sum_i \frac{W_i^2 U_i^2}{\omega(x_i)} - 2b^2 \sum_i \frac{W_i^2 U_i V_i}{\omega(x_i)} -$$

$$b\left[\sum_i W_i U_i^2 - \sum_i \frac{W_i^2 V_i^2}{\omega(x_i)}\right] + \sum_i W_i U_i V_i = 0 \ ,$$

where: $U_i = X_i - \overline{X}$, $V_i = Y_i - \overline{Y}$,

X_i and Y_i are the observed values,

$$\overline{X} = \sum_i \frac{W_i X_i}{\sum_i W_i} \ , \quad \overline{Y} = \sum_i \frac{W_i Y_i}{\sum_i W_i} \ ,$$

$$\omega(x_i) = \text{the weight of } X_i = \frac{1}{\sigma_x^2} \ ,$$

$$\omega(y_i) = \text{the weight of } Y_i = \frac{1}{\sigma_y^2} \ ,$$

and $$W_i = \frac{\omega(x_i)\omega(Y_i)}{b^2\omega(y_i) + \omega(x_i)} \ .$$

The cubic equation was solved using the Newton-Raphson method for finding the root of f(x) (Kelly, 1967):

$$x_{n+1} = x_n - \frac{f(x_n)}{f'(x_n)} \ ,$$

where: $f(x_n)$ = the cubic equation,

$f'(x_n)$ = the derivative of the cubic equation.

After the slope, b, is found the y-intercept, a, is given by:

$$a = \overline{Y} - b\overline{X} \ .$$

The error (σ) was calculated by a Monte Carlo simulation, randomly varying the individual data points according to their calculated uncertainties for at least 20 trials, and calculating the slope (b_r) for each randomized set of data points:

$$\sigma_m = \left[\sum_i \frac{(b_r - b)^2}{N_m} \right]^{\frac{1}{2}}, \quad \sigma_p = \left[\sum_i \frac{(b_r - b)^2}{N_p} \right]^{\frac{1}{2}},$$

where: N_m = no. of random slopes < b_{calc},

N_p = no. of random slopes > b_{calc}.

The age of the sample was calculated using the formula:

$$T = \tau_{230} \ln(1-b),$$

where: $\tau_{230} = \frac{t_{1/2}}{\ln 2} = \frac{75{,}400 \text{ yrs}}{\ln 2} = 108{,}490 \text{ yrs}$,

b = calculated slope.

A one standard deviation error on the age is then calculated using the equation:

$$\sigma_+ = T + \tau_{230} \ln (1-b+\sigma_m),$$

$$\sigma_- = -\tau_{230} \ln (1-b-\sigma_p) - T.$$

RESULTS

Introduction

Samples were collected in Lassen Volcanic National Park (LVNP) during the summers of 1980, 1981, and 1982. The rocks are typical calc-alkaline porphyritic dacites and rhyodacites (table 5) and contain complex phenocryst assemblages. Plagioclase, commonly of two populations, is the dominant phenocryst phase. Mafic phenocrysts present include augite, hypersthene, hornblende, biotite, and magnetite. Hornblende and biotite typically show varying degrees of oxidation and replacement by magnetite and pyroxene. Mafic inclusions, thought to be blobs of basaltic magma quenched upon intrusion into cooler silicic magma (Heiken and Eichelberger, 1980), are abundant in many flow units.

Geologic Setting

Lassen Volcanic Center (LVC) is located in the southernmost part of the Cascade Range, California (fig. 6). LVC consists of an andesitic composite volcano with associated silicic rocks. LVC is surrounded by contemporaneous basalts. The history of LVC can be represented by three stages (Clynne, 1983). Stages I and II cover the growth of the andesitic composite cone, Brokeoff Volcano, from 0.6 to 0.35 m.y. Stage III marks a shift in location and character

TABLE 5

CHEMICAL ANALYSES OF LASSEN VOLCANIC CENTER ROCKS

[Modified after M. A. Clynne, 1983. Oxides adjusted to sum to 100 precent without water. FeO = total iron. Major element composition of UTh-144 equivalent to that of UTh-145].

Analysis number	1	2	3	4	5	7	8
Sample number	DB70	C670A	C1811	C0534	C1706	F78	B9121
Lab number	UTh-122	UTh-145	UTh-142	UTh-84	M148410	UTh-80	UTh-121
SiO_2	69.60	68.84	70.46	69.45	67.50	66.41	60.60
Al_2O_3	15.44	16.04	15.31	16.04	16.45	16.26	17.42
FeO	2.70	2.88	2.50	2.56	3.26	3.90	5.06
MgO	1.14	1.38	1.31	1.06	1.66	2.30	4.05
CaO	2.97	3.54	3.11	2.79	3.79	4.52	6.29
Na_2O	4.35	4.19	4.12	4.23	4.18	3.44	4.15
K_2O	3.12	2.57	2.67	3.25	2.53	2.34	1.57
TiO_2	0.48	0.38	0.36	0.46	0.44	0.60	0.59
P_2O_5	0.12	0.12	0.11	0.11	0.12	0.13	0.17
MnO	0.07	0.06	0.05	0.05	0.06	0.08	0.09
FeO/MgO	2.37	2.09	1.91	2.42	1.96	1.69	1.25

TABLE 5 Chemical Analyses--Continued

Analysis number Sample number Lab number	9 C1724 UTh-143	10 C1660 UTh-150	11 C1736 UTh-62	12 C1731 UTh-64	13 C1844 UTh-134	14 C1840 UTh-113	15 C1843 UTh-129	16 C1661 UTh-83
SiO_2	71.04	69.83	69.53	70.42	56.38	64.83	59.34	68.30
Al_2O_3	15.72	15.63	15.79	15.60	18.72	16.81	18.23	15.84
FeO	2.23	2.56	2.53	2.44	6.82	3.93	5.35	3.15
MgO	0.96	1.48	1.48	1.21	4.33	2.62	4.18	1.72
CaO	2.61	3.20	3.30	2.93	8.82	4.92	6.85	3.94
Na_2O	4.10	4.04	4.17	4.13	3.04	4.00	3.75	3.95
K_2O	2.84	2.76	2.69	2.75	0.98	2.18	1.50	2.51
TiO_2	0.33	0.36	0.36	0.36	0.68	0.51	0.63	0.41
P_2O_5	0.11	0.10	0.10	0.11	0.12	0.13	0.14	0.11
MnO	0.05	0.05	0.05	0.05	0.11	0.07	0.09	0.06
FeO/MgO	2.32	1.73	1.71	2.02	1.58	1.50	1.28	1.83

TABLE 5 Chemical Analyses--Continued

Analysis number Sample number Lab number	17 C0123 M145760	18 C1726 M150260	19 C1728D M150261	20 C1727 M150262	21 C1734 M150264	22 C1765 M150265
SiO_2	59.17	70.84	66.47	69.59	69.37	70.51
Al_2O_3	17.70	15.93	16.06	16.24	15.77	15.57
FeO	5.91	2.75	3.69	2.63	2.73	2.37
MgO	3.91	1.42	2.40	1.51	1.39	1.16
CaO	7.21	3.40	4.70	3.26	3.41	2.88
Na_2O	3.51	4.12	3.18	4.11	4.11	4.20
K_2O	1.59	2.73	2.26	2.72	2.68	2.79
TiO_2	0.73	0.38	0.43	0.37	0.37	0.36
P_2O_5	0.17	0.12	0.10	0.11	0.12	0.11
MnO	0.10	0.05	0.07	0.05	0.05	0.05
FeO/MgO	1.51	1.94	1.54	1.74	1.96	2.04

TABLE 5 Chemical Analyses--Continued

Analysis number	23	24	25	26	27	28
Sample number	C0374	C0401	C0436	C0449	C0495	C0537
Lab number						
SiO_2	56.04	51.88	57.50	61.75	59.90	51.37
Al_2O_3	15.61	17.33	17.20	17.09	17.23	17.36
FeO	6.58	8.23	6.63	4.99	5.52	8.39
MgO	8.06	7.11	4.21	3.51	4.19	8.18
CaO	9.07	9.04	7.59	6.08	6.50	9.00
Na_2O	2.81	3.40	3.76	3.63	3.75	3.23
K_2O	0.94	1.08	1.61	1.94	1.78	0.86
TiO_2	0.64	1.22	1.05	0.73	0.81	1.13
P_2O_5	0.14	0.58	0.34	0.19	0.23	0.32
MnO	0.12	0.13	0.11	0.08	0.08	0.16
FeO/MgO	0.82	1.16	1.57	1.42	1.32	1.03

TABLE 5 Chemical Analyses--Continued

Analysis number	29	30	31	32	33	34
Sample number	C1646	C1649	C1706	C1775	C1797	C1828
Lab number						
SiO_2	56.63	51.70	67.50	55.94	58.26	54.56
Al_2O_3	17.70	16.86	16.45	18.07	18.10	16.94
FeO	6.52	8.09	3.26	6.82	5.91	6.44
MgO	5.12	8.71	1.66	4.70	3.89	7.33
CaO	8.04	9.27	3.79	7.74	7.28	9.40
Na_2O	3.49	3.09	4.18	3.48	3.65	3.29
K_2O	1.23	0.85	2.53	1.70	1.75	0.80
TiO_2	0.85	1.02	0.44	1.06	0.82	0.88
P_2O_5	0.30	0.27	0.12	0.37	0.23	0.24
MnO	0.12	0.14	0.06	0.12	0.10	0.11
FeO/MgO	1.27	0.93	1.96	1.45	1.52	0.88

TABLE 5 Chemical Analyses--Continued

Analysis number	35	36	37	38	39	40
Sample number	C1905	C2171	C2172	C2182	C2191	C2192
Lab number						
SiO_2	50.53	54.15	61.62	61.68	61.89	59.64
Al_2O_3	17.79	17.13	17.14	16.90	16.93	17.82
FeO	8.45	7.69	4.75	5.12	5.12	5.29
MgO	8.46	7.08	3.50	3.59	3.51	4.25
CaO	9.82	7.95	6.34	5.94	6.14	7.37
Na_2O	2.89	3.20	3.77	3.65	3.55	3.39
K_2O	0.65	1.30	1.69	2.09	1.88	1.29
TiO_2	1.00	1.04	0.65	0.75	0.71	0.70
P_2O_5	0.25	0.32	0.19	0.20	0.18	0.19
MnO	0.16	0.13	0.08	0.08	0.09	0.09
FeO/MgO	1.00	1.09	1.36	1.43	1.46	1.24

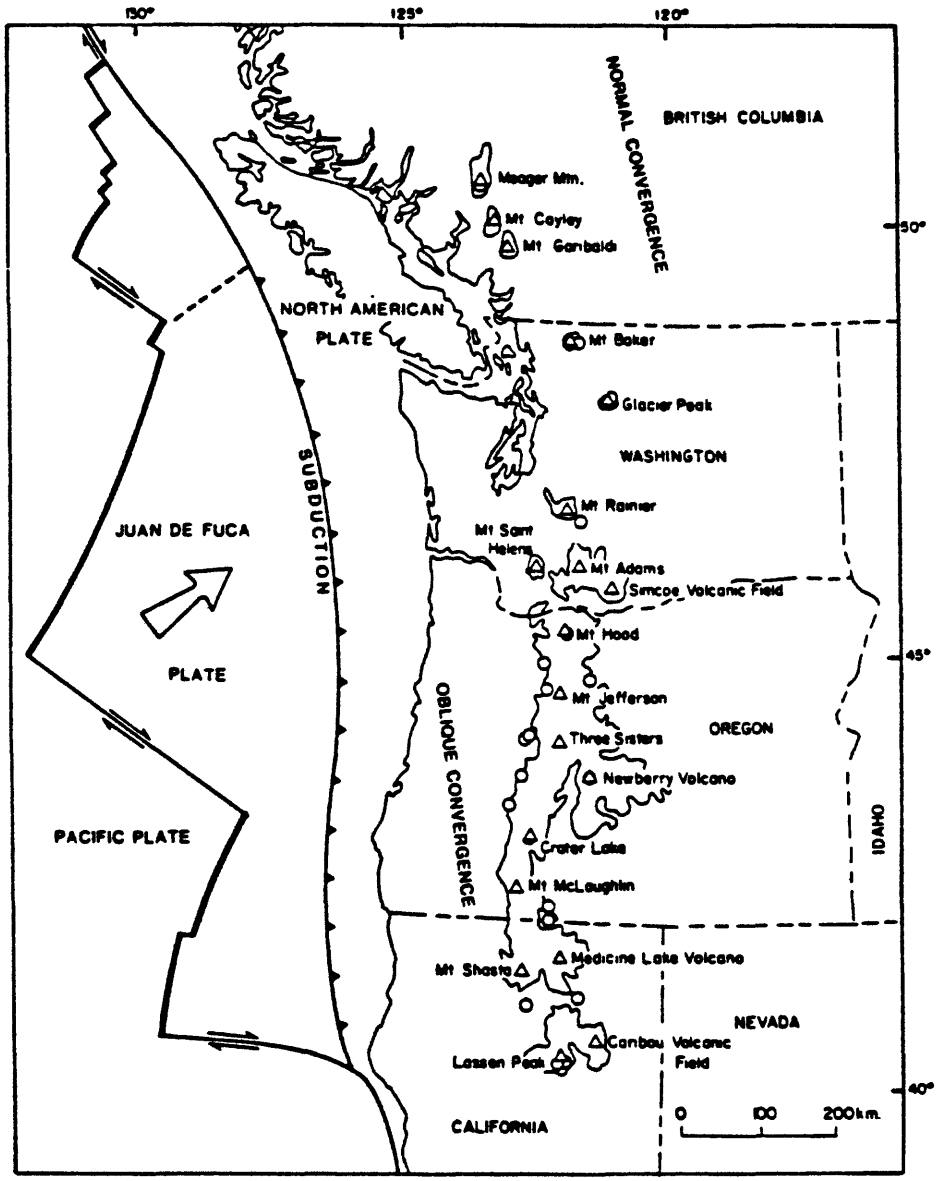

Figure 6. Location and tectonic setting of the Lassen Volcanic Center (after Clynne, 1983). Arrow indicates the direction of plate convergence, and Quaternary volcanic rocks are outlined.

of volcanism. Stage III is represented by the Rockland Tephra, the Lassen dome field, and hybrid rocks.

The Lassen dome field is located on the northeastern flank of the Brokeoff Volcano (figs. 7 and 8) and consists of three groups of rocks: the Bumpass Dacites, the Loomis Rhyodacites, and the Lassen Rhyodacites. The Bumpass Dacites are located in the southeastern end of the Lassen dome field and were emplaced as a series of domes and thick flows. K-Ar ages suggest that the Bumpass Dacites erupted over the interval 0.25 to 0.2 m.y. ago (G. B. Dalrymple, 1982, written commun.). The Loomis Rhyodacites consist of a group of at least 7 thick lava flows and associated pyroclastic deposits erupted from a vent now covered by Lassen Peak (Williams, 1932). The Loomis Rhyodacites are glaciated and therefore are inferred to be at least 20,000 years old. The Lassen Rhyodacites consist of domes and associated pyroclastic deposits located in the western part of the Lassen dome field. Some of the Lassen Rhyodacites are glaciated, but others are post-glacial. The only radiometric age controls currently available on Lassen Rhyodacites are radiocarbon ages of about 1050 years B. P. on charcoal from the Chaos Crags pyroclastic flows.

Historic activity in the Lassen region includes 1850-1851 eruption of Cinder Cone and the 1915 eruption of Lassen Peak. These eruptions produced hybrid lavas belonging to the Twin Lakes Sequence of Clynne (1983), which are mixtures of silicic magma from the Lassen system and magma similar to that of the surrounding regional basalts.

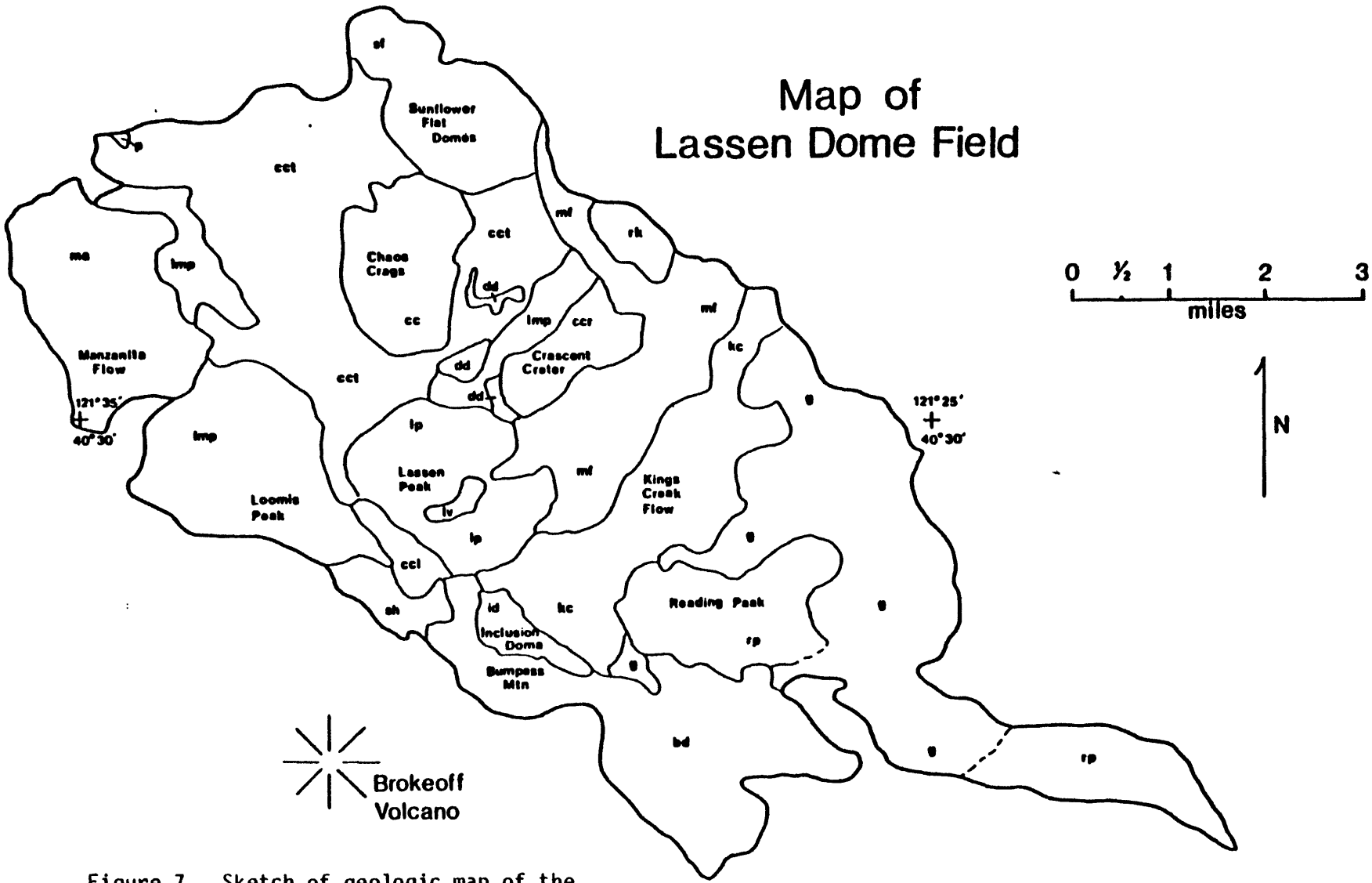

Figure 7. Sketch of geologic map of the Lassen Dome Field. See figure 8 for explanation.

MAP UNITS

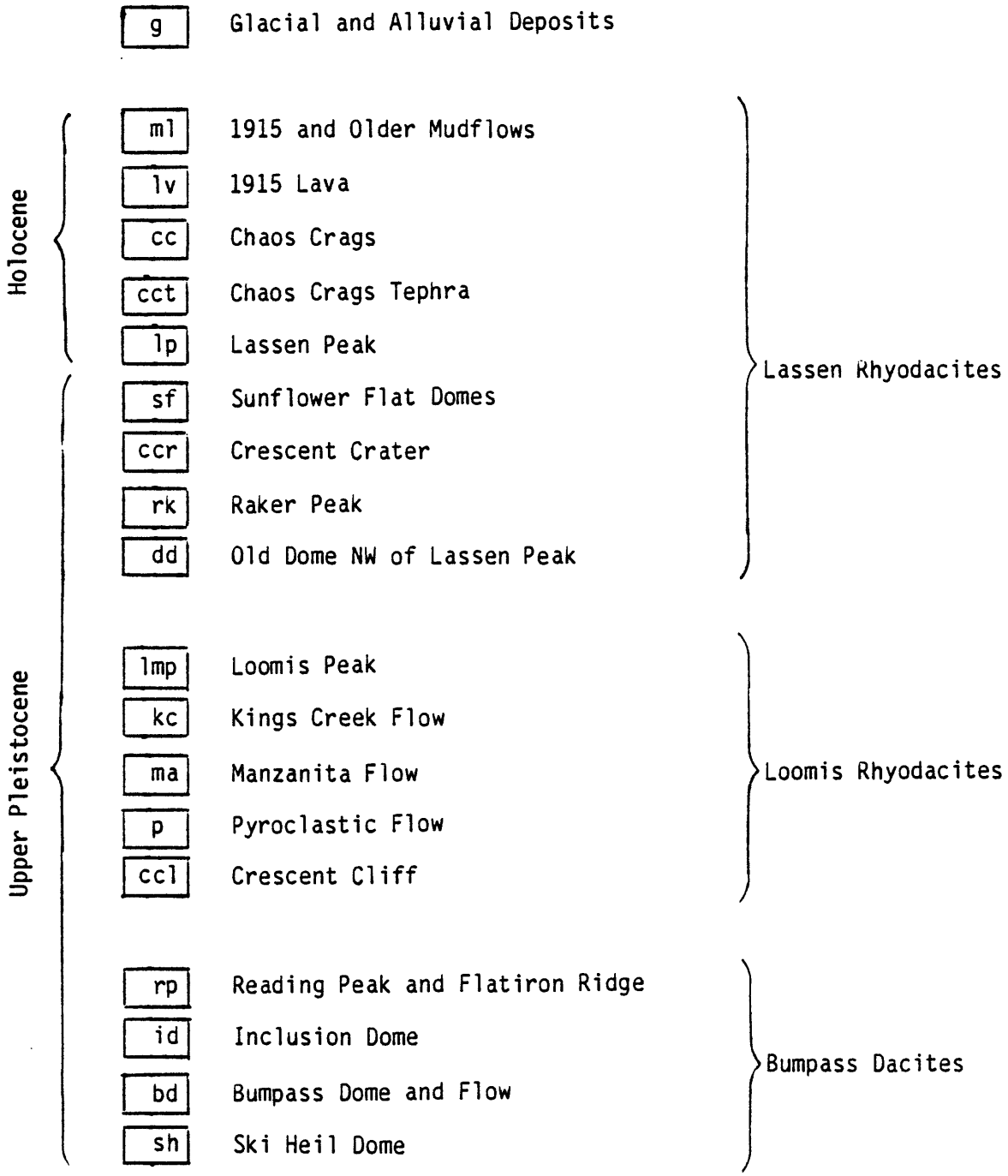

Figure 8. Explanation of units on figure 7.

Deposits of at least 5 glacial advances have been recognized in LVNP (Crandell, 1972; Kane, 1982). Glaciation of pre-Tahoe age occurred approximately 130,000 years B. P. Tahoe glaciation occurred during the interval between 45,000 and 60,000 years B. P. Tioga-age glaciation consists of three separate advances at 29,000-25,000, 25,000-11,000, and 11,000-9,000 years B. P. Most glacial deposits are poorly correlated to particular glacial advances.

Unit Descriptions

Brief petrographic descriptions of the rocks analysed are included to furnish an understanding of the problems encountered in analysis and to provide some basis for interpretation of the data obtained. Phenocrysts are listed in order of decreasing abundance. Microphenocrysts of magnetite are common in all of the rocks. Appendix 2 gives localities for samples in tables 6 and 7.

Dacite of Inclusion Dome

The Dacite of Inclusion Dome contains 10 percent phenocrysts in a devitrified hyalopilitic groundmass. Plagioclase is the only abundant phenocryst; hornblende, hypersthene, augite, biotite, quartz, and olivine are present in minor amounts. Microphenocrysts of magnetite are common. The hornblende and biotite phenocrysts are strongly resorbed and partially to completely replaced by magnetite

and pyroxene. Two populations of plagioclase are present, one being strongly sieved and the other showing no sign of sieving.

Mafic inclusions, ranging in size from 3 mm to 50 cm, are abundant. Typically, the inclusions consist of a felted network of plagioclase and hornblende with abundant microvesicles and clear interstitial glass. Phenocrysts are sparse and probably represent phenocrysts incorporated from the host magma.

Loomis Rhyodacites

Rhyodacite of Loomis Peak. The Rhyodacite of Loomis Peak is a slightly pumiceous, medium-grey, glassy, porphyritic rhyodacite containing 15 percent phenocrysts of plagioclase, hornblende, and hypersthene with sparse biotite in a clear, light-brown, holohyaline groundmass. The plagioclase phenocrysts consist of two populations; euhedral crystals with normal zoning are more common than strongly sieved crystals with clear overgrowth rims. Mafic inclusions reaching 1 m in size are locally abundant. The inclusions consist of a wide variety of textural types.

Rhyodacite Pyroclastic Flow. The rhyodacite pyroclastic flow has 10-15 percent phenocrysts of plagioclase, biotite, hornblende, and quartz. Zircon and apatite occur as sparse accessory minerals in the large mafic phenocrysts. The plagioclase crystals tend to be broken but are not sieved. The biotite and hornblende phenocrysts show no sign of oxidation. Mafic inclusions ranging in size from 1 mm to 10 cm are abundant.

Rhyodacite of Kings Creek. The Rhyodacite of Kings Creek has 15-20 percent phenocrysts of plagioclase, biotite, hornblende, quartz, and hypersthene in a light-brown, glassy groundmass. Plagioclase crystals are mostly unsieved. Biotite and hornblende phenocrysts are fresh with little replacement by magnetite. Hypersthene crystals are small (to .5 mm). Mafic inclusions are sparse.

Rhyodacite of Manzanita. The Rhyodacite of Manzanita has a perlitic to pumiceous, light-brown, glassy groundmass, with phenocrysts of plagioclase, nornblende, and biotite. Plagioclase crystals consist of a homogeneous population with some glass inclusions. Hornblende and biotite crystals are fresh with little replacement by magnetite.

Lassen Rhyodacites

Rhyodacite of Crescent Crater. The Rhyodacite of Crescent Crater has 15-20 percent phenocrysts of plagioclase, hornblende, hypersthene, biotite, and sparse augite in a dense glassy groundmass. The plagioclase is of two populations; phenocryst plagioclase is strongly sieved, whereas groundmass plagioclase is fresh. Hornblende and biotite phenocrysts are strongly oxidized, and replacement by pyroxene and magnetite is common. Splotchy devitrification of the groundmass is common, especially around phenocrysts. Mafic inculsions are abundant.

Rhyodacite of Sunflower Flat. The Rhyodacite of Sunflower Flat has plagioclase, hypersthene, hornblende, augite, and biotite phenocrysts in a dense, light-brown, glassy groundmass. Plagioclase crystals are strongly sieved. Biotite is partially replaced by hornblende and magnetite. Small mafic inclusions are sparse.

Rhyodacite of Lassen Peak. The Rhyodacite of Lassen Peak has plagioclase, biotite, hornblende, quartz, and augite phenocrysts in a devitrified, light-gray groundmass. Most of the plagioclase crystals are sieved and have abundant glass inclusions. Biotite phenocrysts are partially replaced by hornblende and magnetite. Quartz phenocrysts are up to 2 mm in diameter and are rounded. Mafic inclusions are abundant and include a variety of textural types and sizes.

Rhyodacite of Chaos Crags. The Rhyodacite of Chaos Crags has 25-30 percent phenocrysts of plagioclase, hornblende, biotite, quartz, and pyroxene in a light-brown, devitrified groundmass. There are two populations of plagioclase phenocrysts, with unsieved crystals dominant over sieved crystals. The hornblende and biotite crystals are oxidized and partially replaced by magnetite. Pyroxene is sparse and may be from disaggregated mafic inclusions. Mafic inclusions range in size from 1 mm to 10 cm and are abundant. Typically, the inclusions are porphyritic; they contain plagioclase, hornblende, biotite, and quartz xenocrysts.

Pyroclastic Flows of Chaos Crags. The pyroclastic flows of Chaos Crags have the same mineralogy as the Chaos Crags domes. However, plagioclase phenocrysts tend to be unsieved, and hornblende and biotite are unoxidized.

1915 Lava. The dacite lava of the 1915 eruption of Lassen Peak has plagioclase, quartz, hornblende, biotite, and olivine phenocrysts in a dense groundmass of brown glass and microlites of plagioclase, augite, and hypersthene. There are two populations of plagioclase, with unsieved crystals dominant over sieved crystals. The quartz crystals tend to be rounded and cracked. The biotite phenocrysts are slightly oxidized, and many are rimmed with magnetite. Hornblende is partially replaced by hypersthene and magnetite. Olivine crystals tend to be corroded and cracked and are commonly rimmed by pyroxene. Mafic inclusions ranging in size from 1 cm to 50 cm are abundant. They are sparsely porphyritic fine-grained rocks with abundant tiny vesicles. Mafic inclusions contain sparse phenocrysts of calcic plagioclase and olivine, and a variety of phenocrysts from the host are present.

Isochrons

U/Th disequilibrium dating was attempted on 5 rhyodacites from the Lassen dome field (table 6). The criteria used in selecting rocks for dating were estimated age, based on field relationships and previous work, mineralogy, and freshness. At least 2 datable

TABLE 6

ANALYSES FOR URANIUM AND THORIUM CONCENTRATIONS AND ISOTOPIC DATA ON DATED ROCKS

SAMPLES	U (ppm)	Th (ppm)	Th/U	$\frac{230Th}{232Th}$	$\frac{238U}{232Th}$	AGE $\times 10^3$ yrs	$\left(\frac{230Th}{232Th}\right)_o$
UTh-64 Lassen Peak							
whole rock	2.30 ± 0.08	6.72 ± 0.08	2.92 ± 0.11	1.078 ± 0.019	1.037 ± 0.046	3.6 ± 30.9	1.087 ± 0.044
pyroxene	0.18 ± 0.02	0.72 ± 0.03	4.08 ± 0.40	1.096 ± 0.062	0.774 ± 0.074		
magnetite	0.87 ± 0.01	2.05 ± 0.07	2.35 ± 0.07	1.113 ± 0.042	1.129 ± 0.042		
UTh-84 Manzanita							
whole rock	3.47 ± 0.08	9.60 ± 0.21	2.77 ± 0.09	1.127 ± 0.033	1.095 ± 0.046	36.0 ± 32.6	1.114 ± 0.044
magnetite	0.37 ± 0.01	1.45 ± 0.09	3.91 ± 0.27	1.150 ± 0.095	0.775 ± 0.055		
hornblende	0.19 ± 0.04	1.15 ± 0.11	6.12 ± 1.51	0.884 ± 0.126	0.496 ± 0.123		
glass	4.26 ± 0.14	12.65 ± 0.13	2.97 ± 0.10	1.078 ± 0.015	1.021 ± 0.044		
UTh-142 Kings Creek							
whole rock	3.03 ± 0.03	8.79 ± 0.05	2.90 ± 0.03	1.072 ± 0.009	1.045 ± 0.018	50.8 ± 57.0	1.095 ± 2.710
magnetite	0.98 ± 0.01	2.89 ± 0.05	2.94 ± 0.06	1.097 ± 0.025	1.030 ± 0.026		
plagioclase	0.33 ± 0.02	0.79 ± 0.16	2.39 ± 0.50	1.185 ± 0.312	1.271 ± 0.271		
UTh-143 Pyroclastic Flow							
whole rock	3.37 ± 0.02	9.72 ± 0.04	2.88 ± 0.02	1.066 ± 0.007	1.051 ± 0.012	57.0 ± 10.9	1.076 ± 0.149
magnetite	1.29 ± 0.02	6.84 ± 0.14	5.28 ± 0.14	0.871 ± 0.027	0.574 ± 0.019		
UTh-150 Sunflower Flat							
whole rock	3.12 ± 0.05	9.56 ± 0.14	3.07 ± 0.06	1.077 ± 0.022	0.988 ± 0.031	35.3 ± 26.0	1.035 ± 0.353
magnetite	1.12 ± 0.03	3.25 ± 0.05	2.89 ± 0.09	1.025 ± 0.021	1.048 ± 0.040		
hornblende	0.39 ± 0.04	1.44 ± 0.03	3.72 ± 0.39	0.986 ± 0.031	0.816 ± 0.087		

phases with sufficient spread in the ($^{230}Th/^{232}Th$) and ($^{238}U/^{232}Th$) ratios are needed to date a rock, however 3 or 4 phases are desirable to reduce uncertainty. Phases analyzed were chosen on the basis of their homogeneity, freshness, and lack of obvious inclusions. Each phase was analyzed for ^{230}Th, ^{232}Th, ^{234}U and ^{238}U. For all samples analyzed, ^{234}U and ^{238}U were found to be in equilibrium ($^{234}U/^{238}U = 1.0 \pm 0.05$).

Plagioclase and biotite were found in most cases to be unsuitable for dating. Plagioclase contains very low abundances of uranium and thorium. The strong negative correlations between uranium and calcium and thorium and calcium in differentiated rock series (figs. 9, 10, and 11) indicate that uranium and thorium substitution for calcium is not extensive in most rock-forming minerals. This is probably due to charge imbalance rather than the large ionic radii of the elements (Harmon and Rosholt, 1982). In addition, biotite may contain titanium in sufficient concentration to make separation of uranium and thorium difficult. The results are low yields and poor counting statistics. In most cases the ($^{230}Th/^{232}Th$) and ($^{238}U/^{232}Th$) values for biotite and plagioclase fall off the isochron.

Large differences between the uranium and thorium yields may produce unreliable data. Low yields resulted in low counting rates and therefore a large error of uncertainty, producing data that are not compatible with the other data sets of the isochron. Samples with counting rates of less than 0.5 counts per minute (cpm) produce large uncertainties and were discarded. Counting rates of 1 cpm or greater gave the best results.

This Study

⧗ Twin Lakes Andesites

▲ Lassen Rhyodacites

● Loomis Rhyodacites

■ Bumpass Dacites

⊠ Inclusions

M. A. Clynne, 1983, written commun.

△ Lassen Rhyodacites

○ Loomis Rhyodacites

× Stage I Andesites of Brokeoff Volcano

⧖ Stage II Andesites of Brokeoff Volcano

□ Lassen Calc-alkaline Basalts and Andesites

Larsen and Gottried, 1960

+ Andesites and Dacites from
Lassen National Volcanic Park

Figure 9. Key to symbols used on variation diagrams.

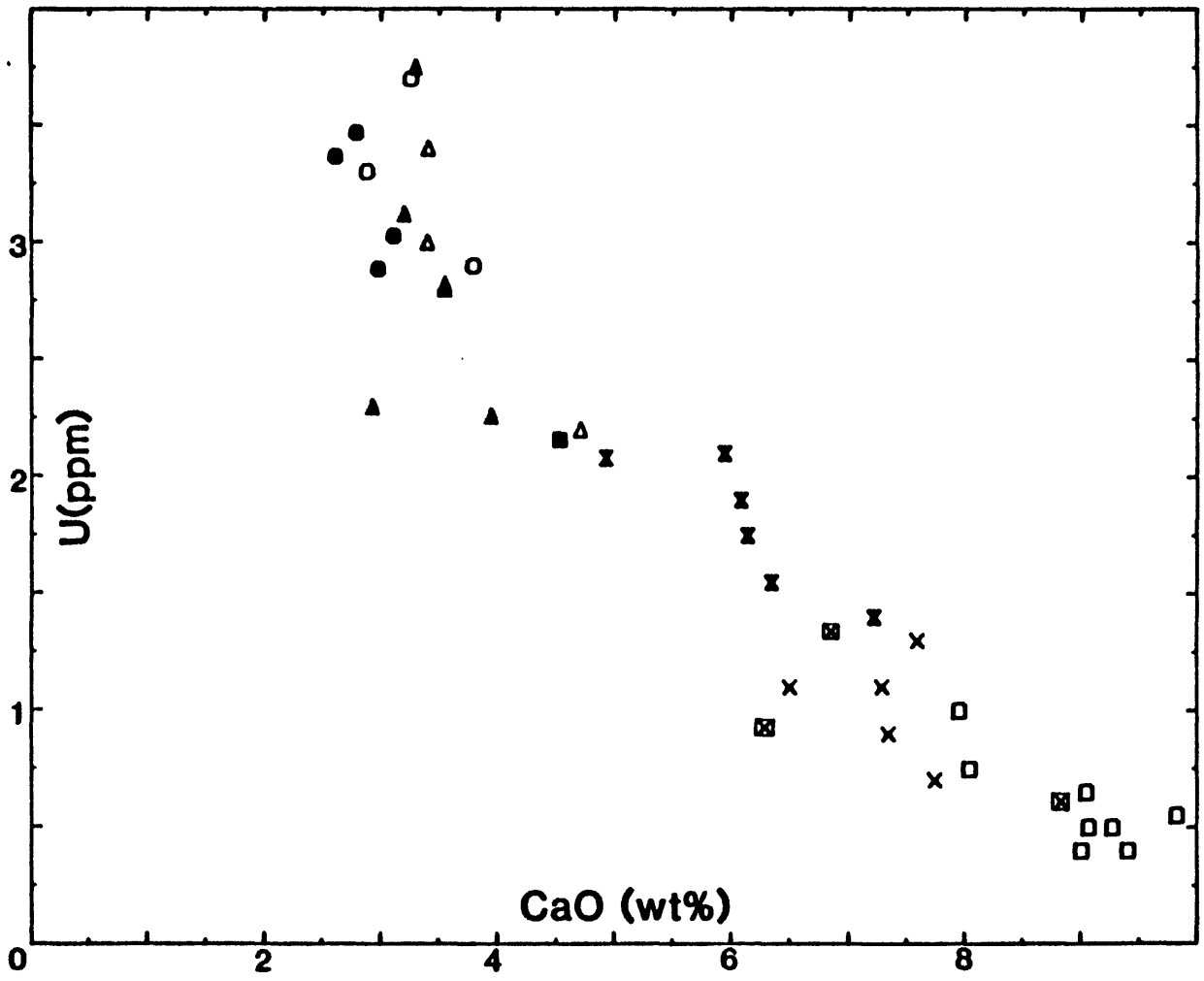

Figure 10. CaO versus U variation diagram. Note the negative correlation between CaO and uranium, with uranium content decreasing with increasing CaO content.

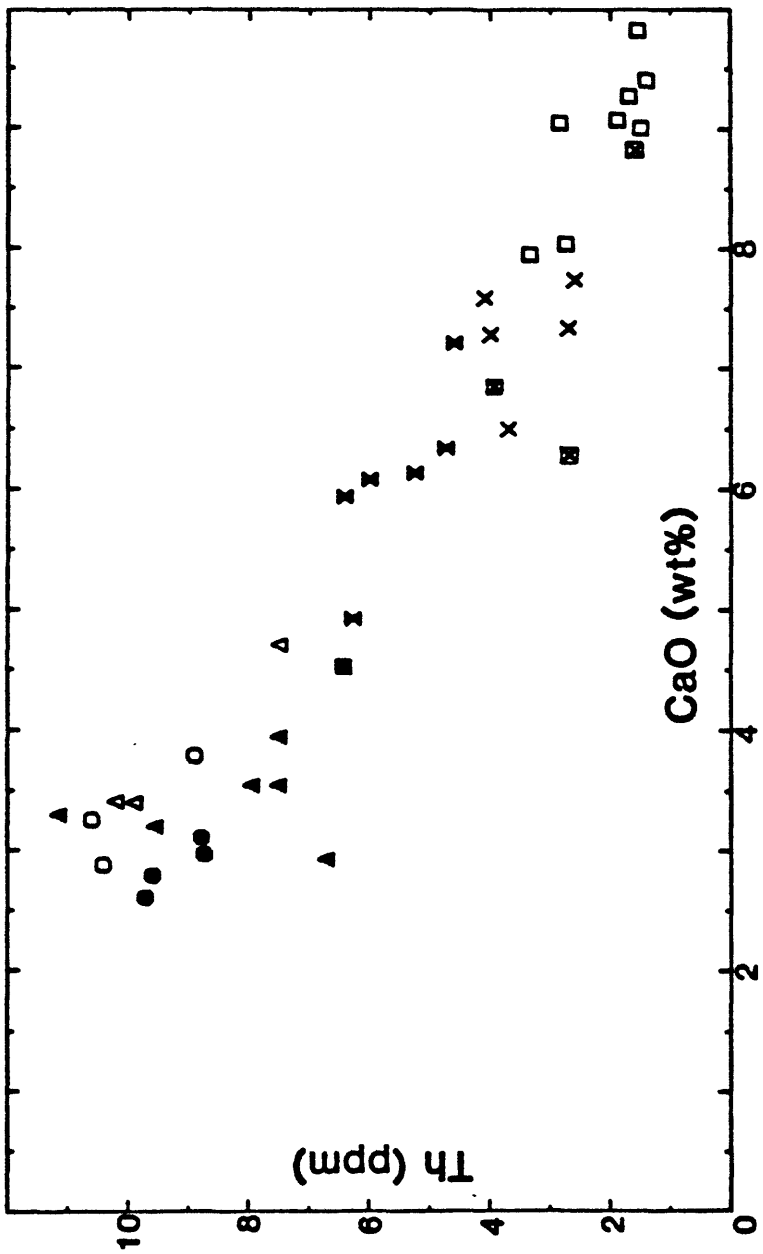

Figure 11. CaO versus Th variation diagram. Note the negative correlation between CaO and thorium, with thorium content decreasing with increasing CaO content.

Fractionation of uranium and thorium between whole rock and mafic phases was variable in the rocks studied, but on the whole fractionation tends to be less than that found by Condomines and others (1982).

Rhyodacite Pyroclastic Flow

A rhyodacitic ash flow deposit of unknown origin from a road cut at the Manzanita Lake, LVNP entrance was dated. A minimum radiocarbon age of >32,000 years B. P. (Crandell and others, 1974) was obtained from charcoal found under the deposit.

Whole-rock, magnetite, and biotite separates were analyzed and yielded an isochron indicating an age of 14,700 + 66,000 - 41,000 years. The biotite is enriched in uranium relative to thorium, perhaps from inclusion of apatite or zircon crystals. Omitting the biotite point from the isochron changes the age to 57,000 ± 10,900 with an initial $^{230}Th/^{232}Th$ ratio of 1.076 ± 0.149 (fig. 12). This is in agreement with preliminary K-Ar age of approximately 50,000 years (A. L. Cook, 1983, oral commun.) and a radiocarbon age of >42,800 years on charcoal found within the ashflow deposit.

Rhyodacite of Kings Creek

The Rhyodacite of Kings Creek is a thick flow originating from a vent now covered by Lassen Peak. The age of the Rhyodacite of Kings Creek is poorly known. The flow was glaciated by Tioga glaciers but evidence for earlier glaciations is lacking. Radiometric ages include a fission track age of <200,000 years (P. A. Bowen, 1983, written commun.) and a preliminary K-Ar age of 30,000 to 50,000

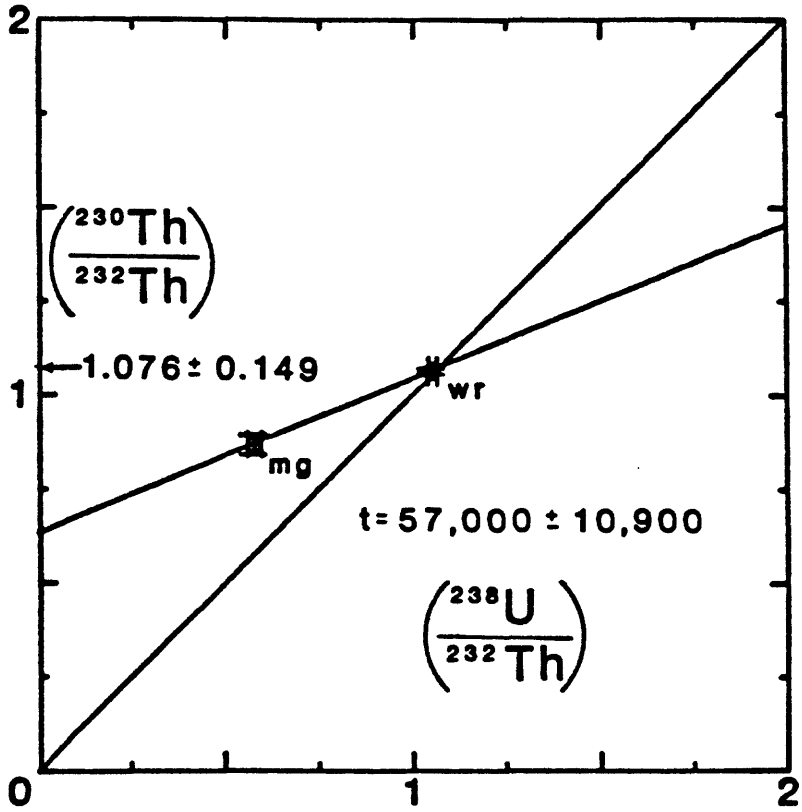

Figure 12. Internal isochron for the Rhyodacite Pyroclastic Flow, with an age of 57,000 ± 10,900 and and initial ($^{230}Th/^{232}Th$) ratio of 1.076 ± 0.149.

years (A. L. Cook, 1983, oral commun.). Peat from fluvial sediments directly below the lava flow yielded a radiocarbon age of 31,280 ± 200 years.

Whole-rock, magnetite, and plagioclase separates were analyzed and yielded an isochron indicating an age of 50,800 ± 57,000 years with an initial $^{230}Th/^{232}Th$ ratio of 1.095 ± 2.710 (fig. 13). The large error on the age and intial ratio are due to the large error on the plagioclase data.

Rhyodacite of Manzanita

The Rhyodacite of Manzanita is a thick lava flow located southwest of Manzanita Lake. The flow is unglaciated and no previous radiometric age date is availiable. Williams (1932) stated that the Rhyodacite of Manzanita is one of the oldest of the Loomis Rhyodacites, whereas Macdonald (1983) suggested that it is very young, perhaps even post-glacial. Recent field work shows that the Rhyodacite of Manzanita predates the Tioga glaciation but is located beyond the limit of icecap glaciation (R. L. Christiansen, 1983, oral commun.).

Whole-rock, magnetite, hornblende, and glass phases from the Rhyodacite of Manzanita yielded an isochron indicating an age of 36,000 ± 32,600 and an initial $^{230}Th/^{232}Th$ ratio of 1.114 ± 0.044 (fig. 14). Biotite and plagioclase were also analyzed, but yielded points off the isochron. Both the plagioclase and biotite have low uranium and thorium concentrations, and poor yields resulted in large errors.

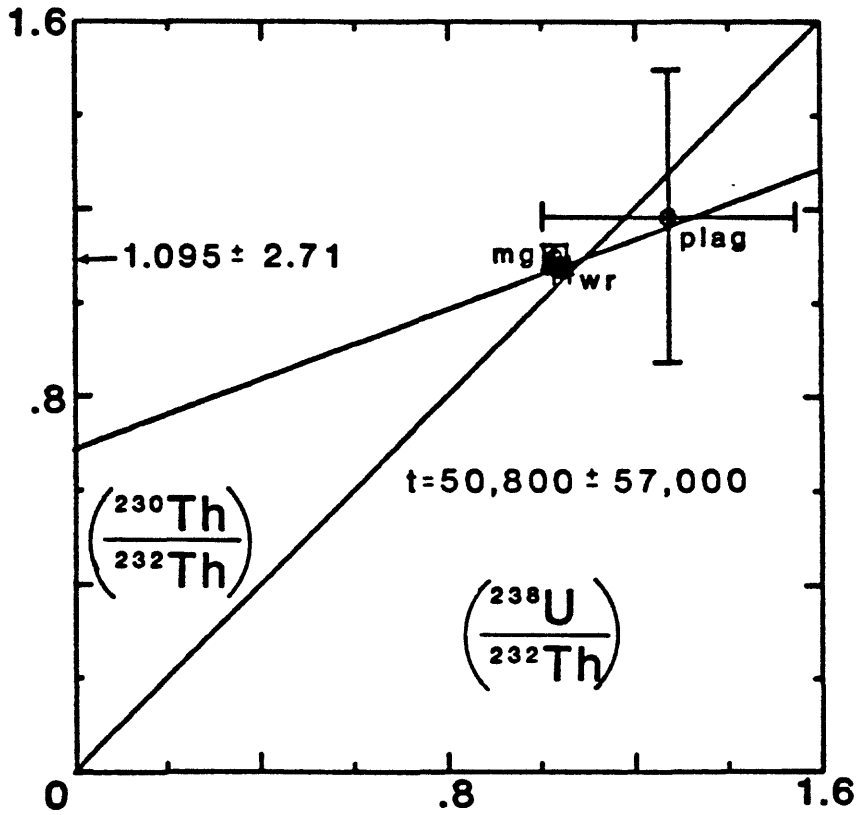

Figure 13. Internal isochron for the Rhyodacite of Kings Creek, with an age of 50,800 ± 57,000 and an initial ($^{230}Th/^{232}Th$) ratio of 1.095 ± 2.71. The large error is due to the uncertainty of the plagioclase data point.

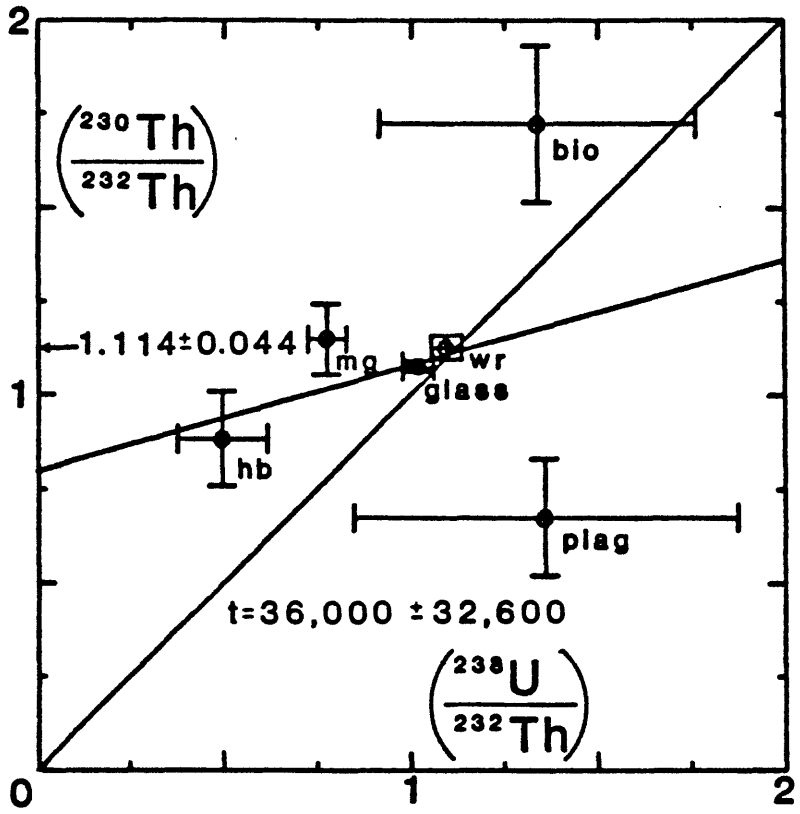

Figure 14. Internal isochron for the Rhyodacite of Manzanita, with an age of 36,000 ± 32,600 and an intitial ($^{230}Th/^{232}Th$) ratio of 1.114 ± 0.044. The plagioclase and biotite points plot off the isochron and were therefore ignored in the calculations.

Rhyodacite of Sunflower Flat

The Rhyodacite of Sunflower Flat is a series of at least seven domes. The domes are unglaciated, although moraines of Tioga age are present along their eastern margin. Glacial evidence suggests that the Sunflower Flat domes are at least 25,000 to 30,000 years old.

Whole rock, magnetite, and hornblende phases analyzed from the Rhyodacite of Sunflower Flat yielded an isochron age of 35,300 ± 26,000 years old with an initial $^{230}Th/^{232}Th$ ratio of 1.035 ± 0.353 (fig. 15). The large error on this date is in large part due to the lack of spread in the data points.

Rhyodacite of Lassen Peak

Lassen Peak is a large rhyodacite dome located in northwestern LVNP. The age of Lassen Peak is unknown. The summit of Lassen Peak is above the snow line (Kane, 1973), but it is covered with autobreccia, indicating that it is unglaciated. Based on a small late Tioga moraine found low on the eastern flank, Crandell (1972) suggested that Lassen Peak is between 8,000 and 11,000 years old. Pyroxene and magnetite mineral separates and a whole rock sample from Lassen Peak were analyzed. An isochron was constructed indicating the age of Lassen Peak to be 3,600 ± 30,000 years, with an initial $^{230}Th/^{232}Th$ ratio of 1.087 ± 0.044 (fig. 16). The data indicates that Lassen Peak is very young, exceeding the limits of this dating method.

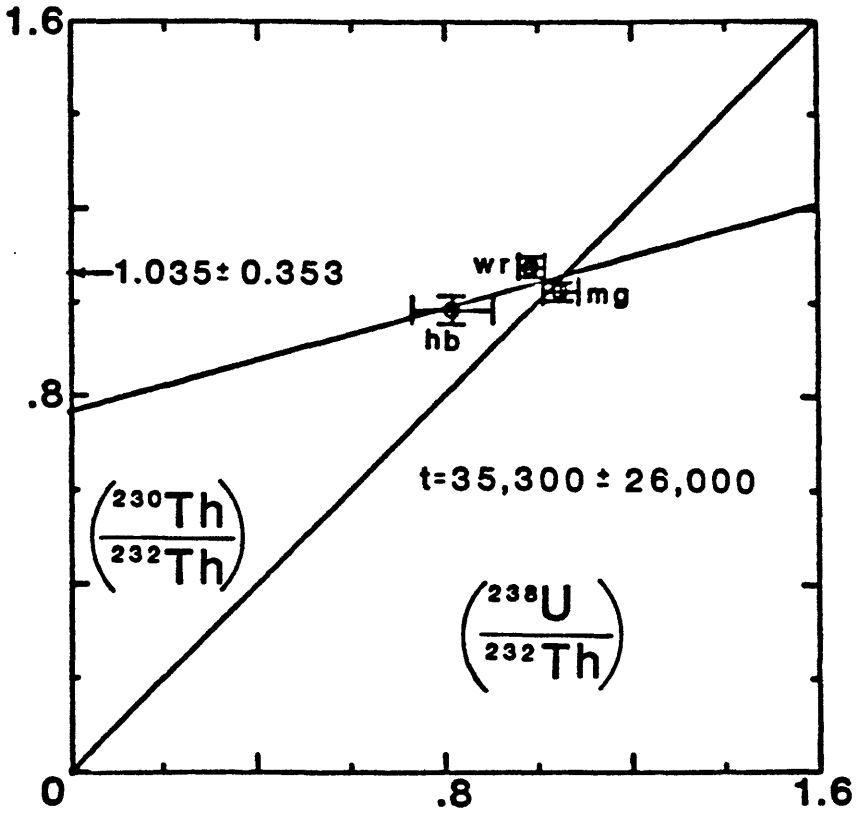

Figure 15. Internal isochron for the Rhyodacite of Sunflower Flat, with an age of 35,300 ± 26,000 and an initial ($^{230}Th/^{232}Th$) ratio of 1.035 ± 0.353.

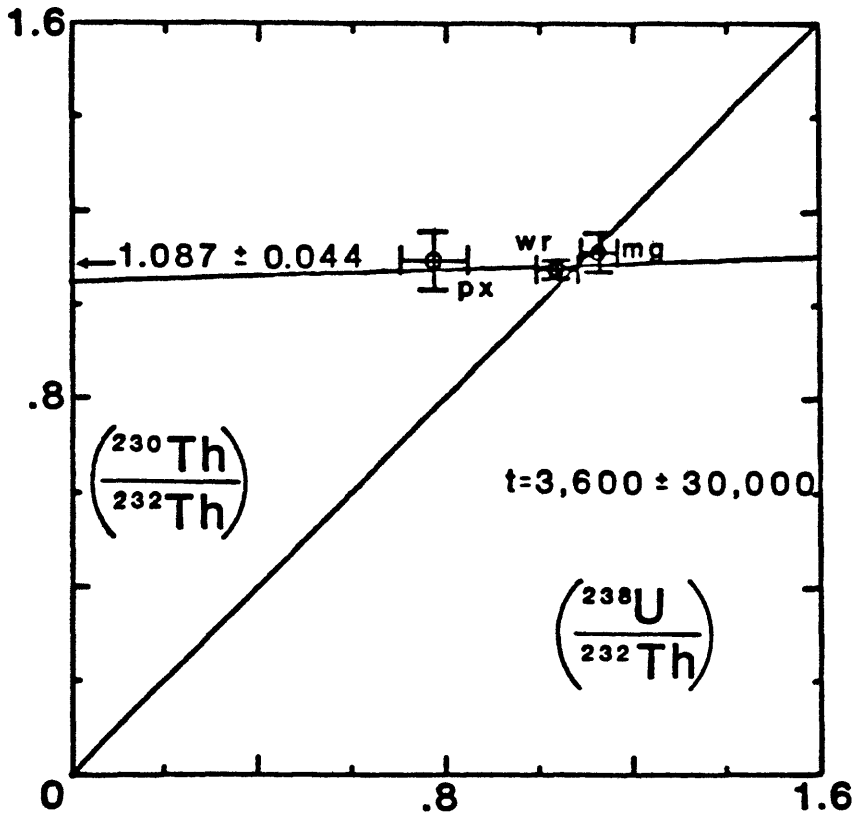

Figure 16. Internal isochron for the Rhyodacite of Lassen Peak, with an age of 3,600 ± 30,000 and an initial ($^{230}Th/^{232}Th$) ratio of 1.087 ± 0.044.

Th/U Ratio Data

Rocks from the Lassen dome field have uranium concentrations ranging from 0.5 to 3.75 ppm and thorium concentrations ranging from 1.4 to 11.1 ppm (tables 6, 7, and 8). Thorium and uranium show the expected trend of enrichment with differentiation (figs. 17 and 18). Values of the Th/U ratio range from 2.7 to 3.3, with an average Th/U ratio of 3.19. A linear relationship between uranium and thorium can be seen on figure 19, with the thorium and uranium data plotting on a line passing through the origin. The increase in uranium and thorium content with increasing SiO_2 may be attributed to fractional crystallization because the partition coefficents for uranium and thorium in early crystallizing minerals are very low (Allegre and Condomines, 1976; Condomines and others, 1981a).

TABLE 7

ANALYSES OF URANIUM AND THORIUM CONCENTRATION AND ISOTOPIC DATA FOR ROCKS NOT DATED

SAMPLES	U (ppm)	Th (ppm)	Th/U	$\frac{^{230}Th}{^{232}Th}$	$\frac{^{238}U}{^{232}Th}$
UTh-62 Crescent Crater whole rock	3.75 ± 0.07	11.16 ± 0.19	2.98 ± 0.08	1.138 ± 0.026	1.018 ± 0.034
UTh-80 Inclusion Dome whole rock	2.16 ± 0.06	6.44 ± 0.10	2.99 ± 0.10	1.091 ± 0.024	1.014 ± 0.038
UTh-83 Chaos Crags whole rock	2.26 ± 0.08	7.51 ± 0.10	3.32 ± 0.13	1.088 ± 0.020	0.915 ± 0.042
UTh-113 "1915" Lava whole rock	2.08 ± 0.02	6.28 ± 0.05	3.01 ± 0.04	1.049 ± 0.013	1.007 ± 0.017
UTh-121 Inclusion Dome Inclusion whole rock	0.93 ± 0.03	2.70 ± 0.06	2.89 ± 0.12	1.061 ± 0.030	1.051 ± 0.049
UTh-122 Loomis Peak whole rock	2.89 ± 0.02	8.74 ± 0.07	3.02 ± 0.04	1.092 ± 0.013	1.003 ± 0.019
UTh-129 "1915" Inclusion whole rock	1.34 ± 0.01	3.95 ± 0.05	2.95 ± 0.05	0.985 ± 0.017	1.027 ± 0.021
UTh-134 Lassen Inclusion whole rock	0.61 ± 0.02	1.59 ± 0.02	2.60 ± 0.10	1.075 ± 0.023	1.167 ± 0.048
UTh-144 Chaos Crags Pyroclastic whole rock	2.80 ± 0.02	7.96 ± 0.06	2.84 ± 0.03	1.067 ± 0.013	1.067 ± 0.019
UTh-145 Chaos Crags Pyroclastic whole rock	2.82 ± 0.01	7.53 ± 0.07	2.67 ± 0.03	1.092 ± 0.015	1.137 ± 0.020

TABLE 8

URANIUM AND THORIUM ANALYSES OF ROCKS FROM THE LASSEN AREA

SAMPLE	U (ppm)	Th (ppm)	Th/U
C0123 Andesite of Bluff Falls	1.4 ± 0.36	4.6 ± 0.09	3.32
C0374 Andesite of Red Lake Mtn.	0.5 ± 0.07	1.9 ± 0.04	3.80
C0401 Quaternary basalt	0.65 ± 0.10	2.85 ± 0.04	4.38
C0436 Andesite of Mill Canyon	1.3 ± 0.07	4.1 ± 0.04	3.15
C0449 Andesite of Mt. Diller	1.9 ± 0.07	6.0 ± 0.06	3.16
C0495 Andesite of Ski Hill	1.1 ± 0.08	3.7 ± 0.07	3.36
C0537 Basalt of Cold Creek Butte	0.4 ± 0.06	1.5 ± 0.05	3.75
C1646 Andesite of Sifford Mtn.	0.75 ± 0.07	2.75 ± 0.06	3.67
C1649 Andesite of Sifford Mtn.	0.5 ± 0.17	1.7 ± 0.07	3.40
C1706 Dacite of Reading Peak	2.9 ± 0.29	8.9 ± 0.09	3.08
C1726 Rhyodacite of Chaos Crags (pf)	3.0 ± 0.09	9.9 ± 0.10	3.31
C1727 Rhyodacite of Sunflower Flat (pf)	3.7 ± 0.15	10.6 ± 0.11	2.90
C1728D Rhyodacite of Kings Creek (pf)	2.2 ± 0.11	7.5 ± 0.08	3.44
C1734 Rhyodacite of Chaos Crags (dome 1)	3.4 ± 0.14	10.2 ± 0.10	2.99
C1765 Rhyodacite of Kings Creek (pf)	3.3 ± 0.13	10.4 ± 0.10	3.19
C1775 Andesite of Rock Spring	0.7 ± 0.11	2.6 ± 0.10	3.71
C1797 Andesite of Ski Hill	1.1 ± 0.08	4.0 ± 0.04	3.64
C1828 Andesite of Red Lake Mtn.	0.4 ± 0.06	1.4 ± 0.04	3.50
C1905 Quaternary basalt	0.55 ± 0.07	1.55 ± 0.09	3.35
C2171 Andesite of Huckleberry Lake	1.00 ± 0.16	3.35 ± 0.05	3.35
C2172 Andesite of Glassburner Meadows	1.55 ± 0.14	4.75 ± 0.05	3.06
C2182 Andesite of Mt. Diller	2.1 ± 0.11	6.4 ± 0.06	3.05
C2191 Andesite of Glassburner Meadows	1.75 ± 0.15	5.25 ± 0.05	3.00
C2192 Andesite of Mill Canyon	0.9 ± 0.11	2.7 ± 0.05	3.00

Analyses by Instrumental Neutron Activation
Analysts: G. A. Wandless and L. J. Schwarz, U. S. Geological Survey, Reston, VA
pf= pyroclastic flow

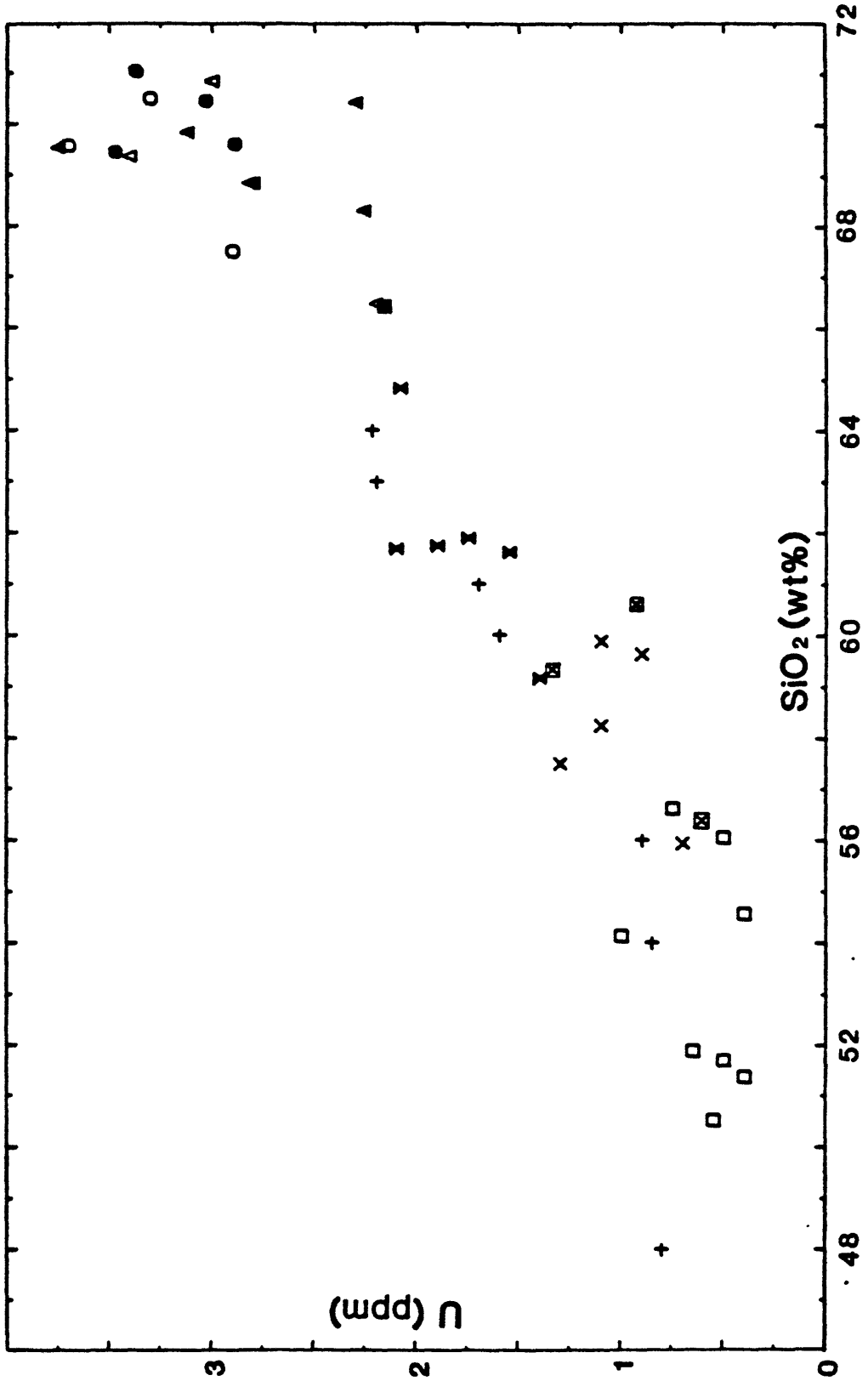

Figure 17. U versus SiO_2 variation diagram. Note the increase in uranium content with differention.

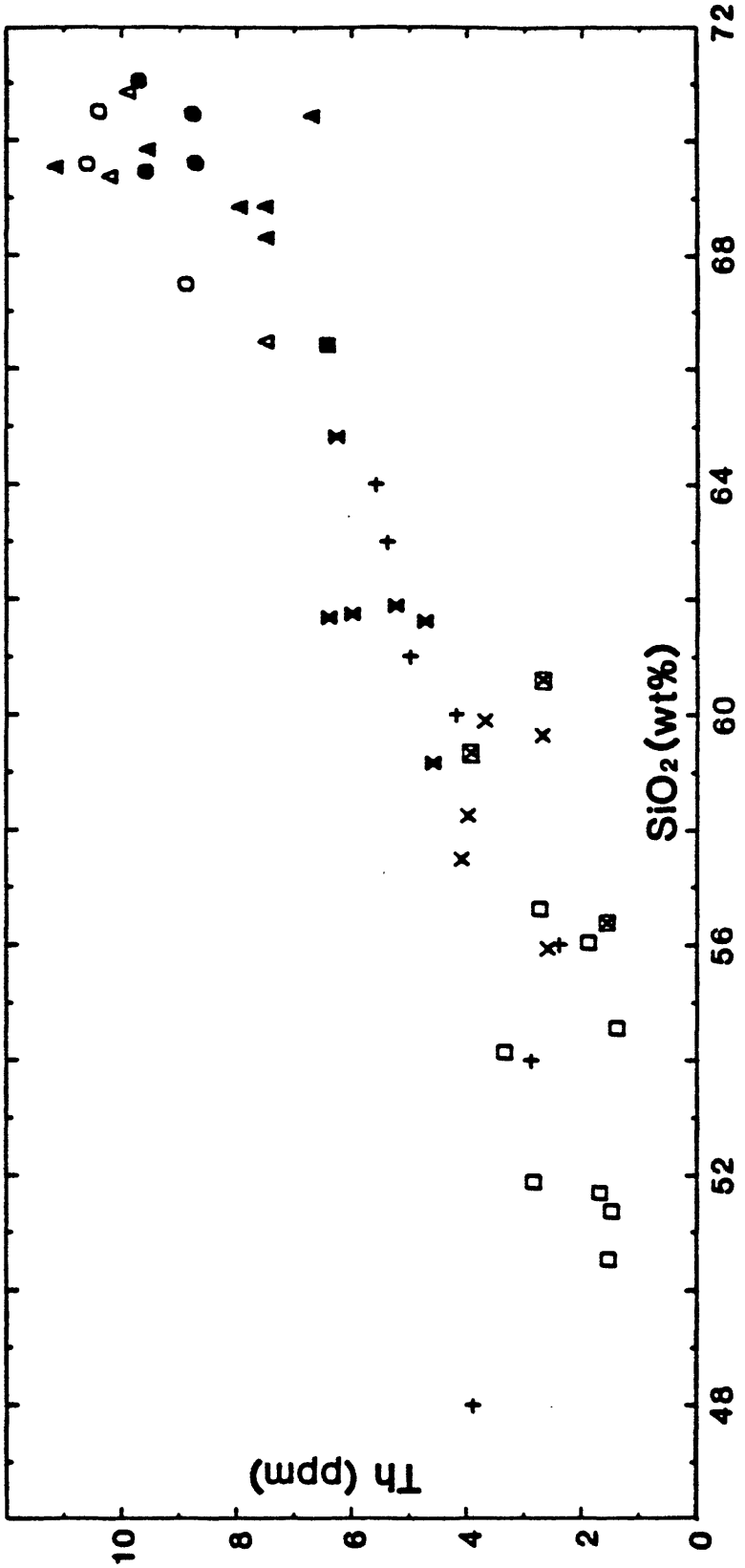

Figure 18. Th versus SiO_2 variation diagram. Note the increase in thorium content with differentiation.

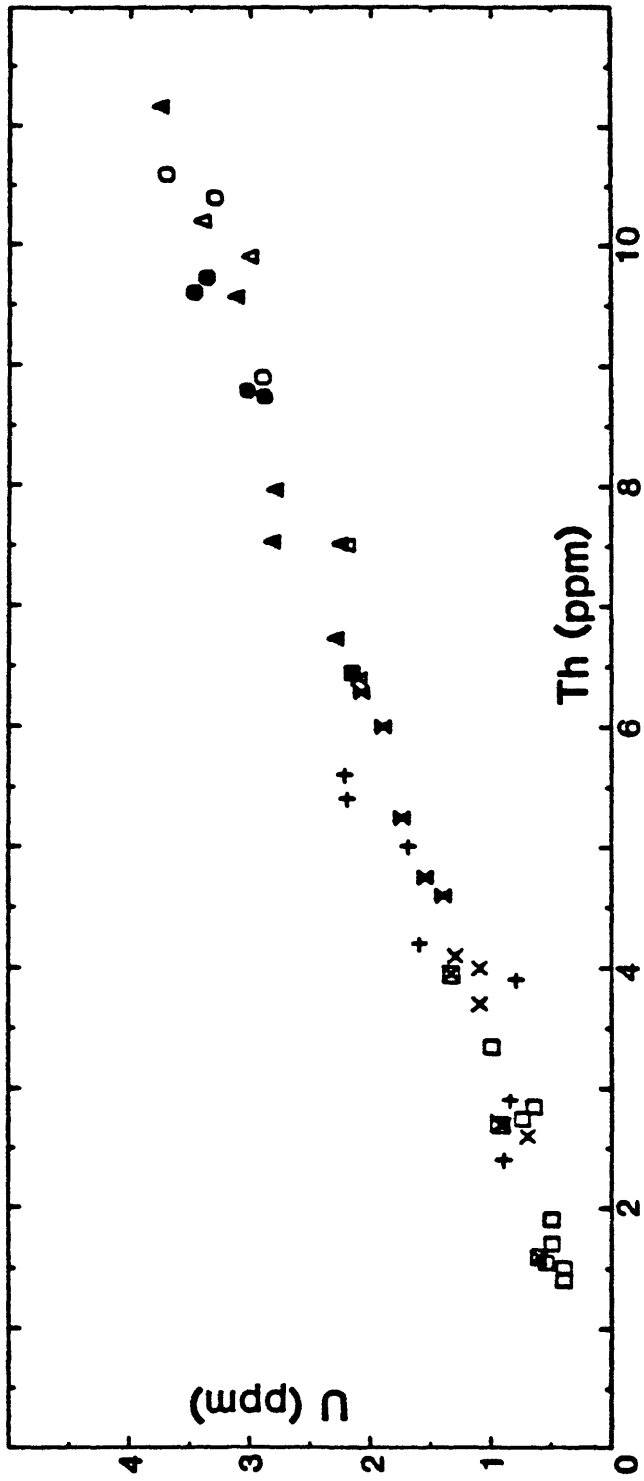

Figure 19. Th versus U variation diagram. Note the linear relationship between thorium and uranium. The average Th/U ratio value is 3.19.

DISCUSSION

Introduction

Clynne (1983) stated that the lavas of the Lassen Volcanic Center are related by crystal fractionation to the regional basaltic magma. The basaltic magmas are probably produced by partial fusion of upper mantle material and modified by crystal fractionation and/or assimilation of crustal material at or near the base of the crust.

Petrographic evidence and major element chemistry suggest that the dominant differentiation process is crystal fractionation. The model proposed by Clynne (1983) for the production of the Lassen Volcanic Center andesites and silicic rocks is open system fractionation with periodic mixing of new mafic parent with the fractionating magma. This is similar to a general model (fig. 20) for calc-alkaline intermediate to silicic rocks proposed by Hildreth (1981).

Partial Melting versus Fractional Crystallization

The uranium and thorium in the mantle source material of basaltic magmas are assumed to be in radioactive equilibrium, $(^{230}Th/^{238}U) = 1$ (Condomines and others, 1982). Although the

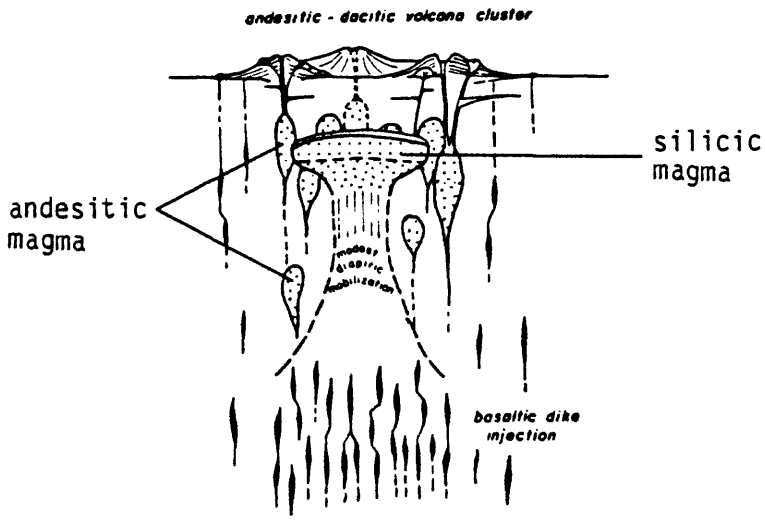

Figure 20. Possible model for the magmatic system of the Lassen Volcanic Center (after Hildreth, 1981). Long-continued injection of basalt into the base, differentiation and rise of intermediate magma produces a zoned system.

origin of U/Th fractionation by partial melting is poorly understood, it must occur, because all recent basaltic lavas plot to the left of the equiline, $(^{230}Th/^{238}U) > 1$ (Allegre and Condomines, 1982). Thus, mafic lavas produced by partial melting are enriched in thorium relative to uranium, and relative to their mantle source. Fractionation of uranium and thorium during partial melting is further supported by conclusions derived from lead isotopic studies (Tatsumoto, 1978).

Uranium and thorium are among the most hygromagmatophile elements, hence the U/Th ratio of the melt remains nearly constant during fractional crystallization (Condomines and Allegre, 1980; Condomines and others, 1982). There is little or no effect on the U/Th ratio until accessory minerals that accept highly incompatible elements begin to crystallize, e.g. apatite, allanite, and sphene (Allegre and Condomines, 1976). These minerals are not present in rocks from the Lassen dome field.

Figure 21 illustrates behavior of uranium and thorium during partial melting and fractional crystallization. S represents a magma source in isotopic equilibrium, M the primary magma, and $I_1, I_2, \ldots I_n$ fractionated lavas erupted in sequence. The open arrows show the isotopic trend produced by partial melting. The black arrows show the isotopic trend produced by fractional crystallization, which with time trends toward isotopic equilibrium. Figure 21a shows magmas with $(^{230}Th/^{238}U)>1$. Figure 21b shows magmas with $(^{230}Th/^{238}U)<1$. This study and others using similar techniques indicate that most young volcanic

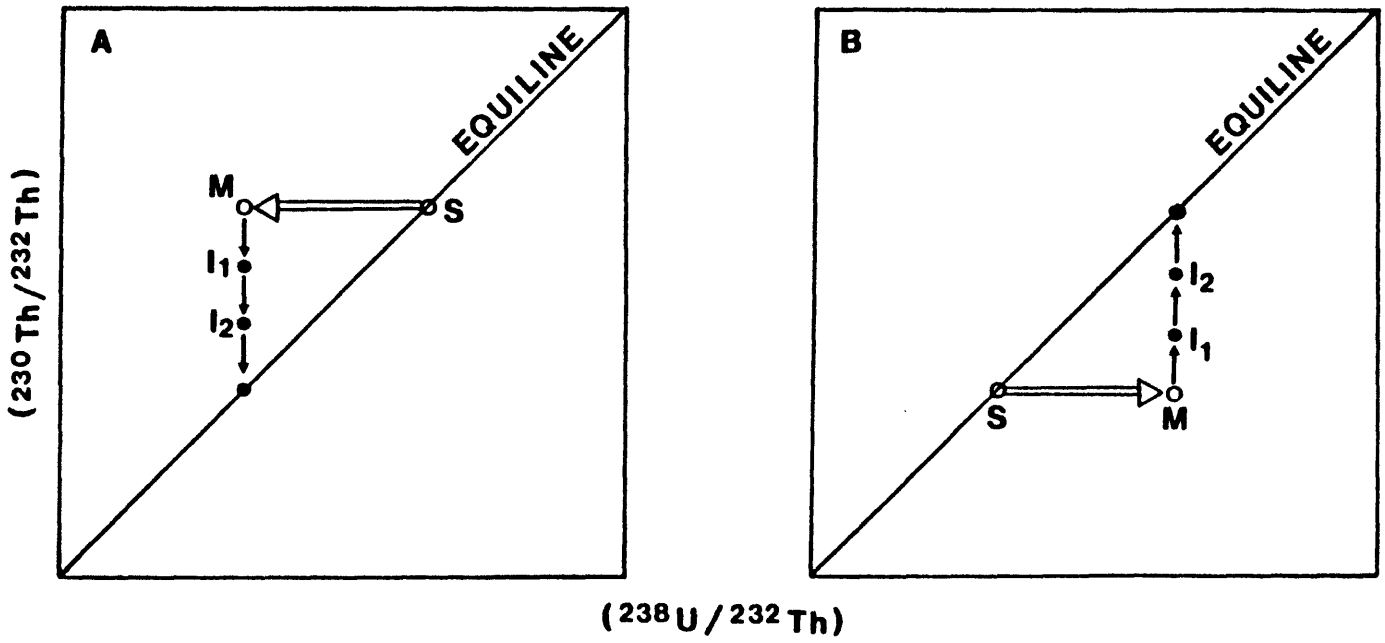

Figure 21. Isochron diagram showing geochemical behavior of the ^{230}Th–^{238}U system during partial melting and fractional crystallization (see text for further explanation). S, magma source; M, primary magma; I_1, I_2, ...I_n, different lavas erupted at different times. Open arrows represent partial melting and solid arrows represent radioactive decay during fractional crystallization (Allegre and Condomines, 1982).

rocks have $(^{230}Th/^{238}U)>1$ (Allegre and Condomines, 1976, 1982; Baranowski and Harmon, 1978; Condomines and others 1976, 1981a, 1981b, 1982; Newman and others, 1981) Figure 21b represents the case in which magmas are preferentially enriched in uranium relative to thorium. This could be the case if the magma source had become enriched in uranium, possibly by mantle metasomatism.

U/Th Isotopic Constraints on the Origin of Lassen Volcanic Center Magmas

^{230}Th and ^{238}U data obtained on rocks from the Lassen dome field plot to the left of the equiline ($(^{230}Th/^{238}U) > 1$) on a ^{230}Th-^{238}U isochron diagram (fig. 22) with only a few exceptions: 1915 inclusion (UTh-129), Lassen Peak inclusion (UTh-134), and Chaos Crags pyroclastic flow (UTh-145). The trend observed at Lassen can be explained in several ways: by depletion of uranium relative to thorium in the differentiating magma chamber, by origin of the rock suite through partial melting of mantle material previously depleted by a partial melting event, or by mixing of Lassen dome field magma with a magma having a higher $(^{230}Th/^{232}Th)$ ratio. The initial $(^{230}Th/^{232}Th)_0$ ratio of the mantle source of the Lassen dome field magma is unknown, therefore, a choice between the above possibilities must be based on other evidence.

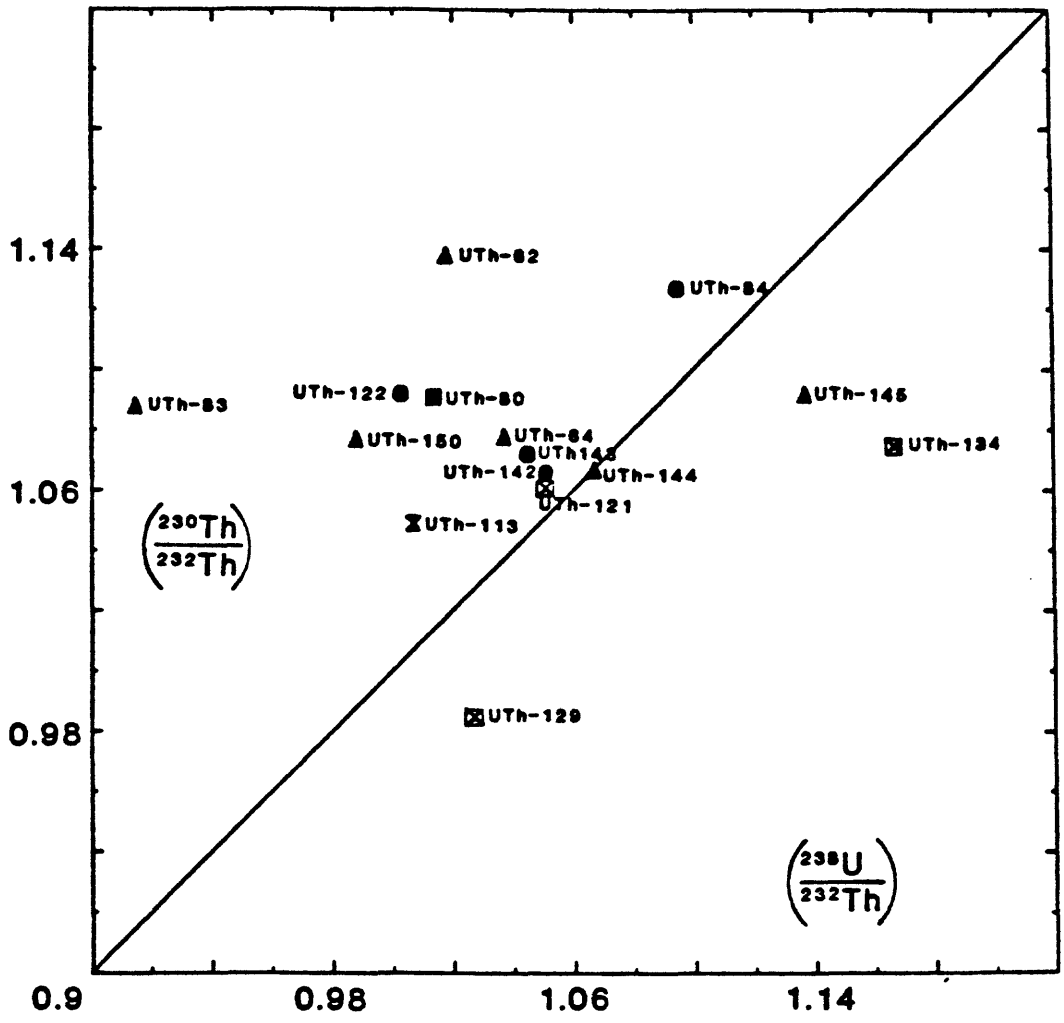

Figure 22. Isochron diagram with whole-rock data plotted showing an expanded view of the samples analyzed in this study and their relative positions.

Average contintenal crust contains 2.7 ppm uranium and 9.6 ppm thorium (Taylor and White, 1966). Partial melting of crustal material would produce magma with even higher uranium and thorium abundances because uranium and thorium are strongly partitioned into the melt phase. Rocks with SiO_2 content similar to those of the Lassen dome field that were derived from sialic crustal material or are interpreted as having assimilated sialic crust nave Th/U ratios similar to those of the rocks of the Lassen dome field, but have uranium abundances greater than 10 ppm and thorium abundances greater than 25 ppm (e.g. Mahood, 1981; Deruelle, 1982). The low whole-rock abundances of uranium and thorium found in the rocks of the Lassen dome field support the interpretation of Clynne (1983) that the parent magmas of the Lassen Volcanic Center rocks are partial melts of mantle material and that assimilation of young, sialic crustal material in the Lassen Volcanic Center is not significant.

There is little variation of the Th/U ratio in rocks from the Lassen Volcanic Center (figs. 19 and 23). This indicates that the observed variation in concentration of uranium and thorium with differentiation is the result of fractional crystallization and not partial melting (Allegre and Condomines, 1976; Condomines and others, 1981a). This supports the findings of Clynne (1983), who suggested that fractional crystallization is the dominant process in the evolution of magmas of the Lassen Volcanic Center.

If it is assumed that fractional crystallization is the dominant process affecting magmas of the Lassen dome field, the observed Th/U

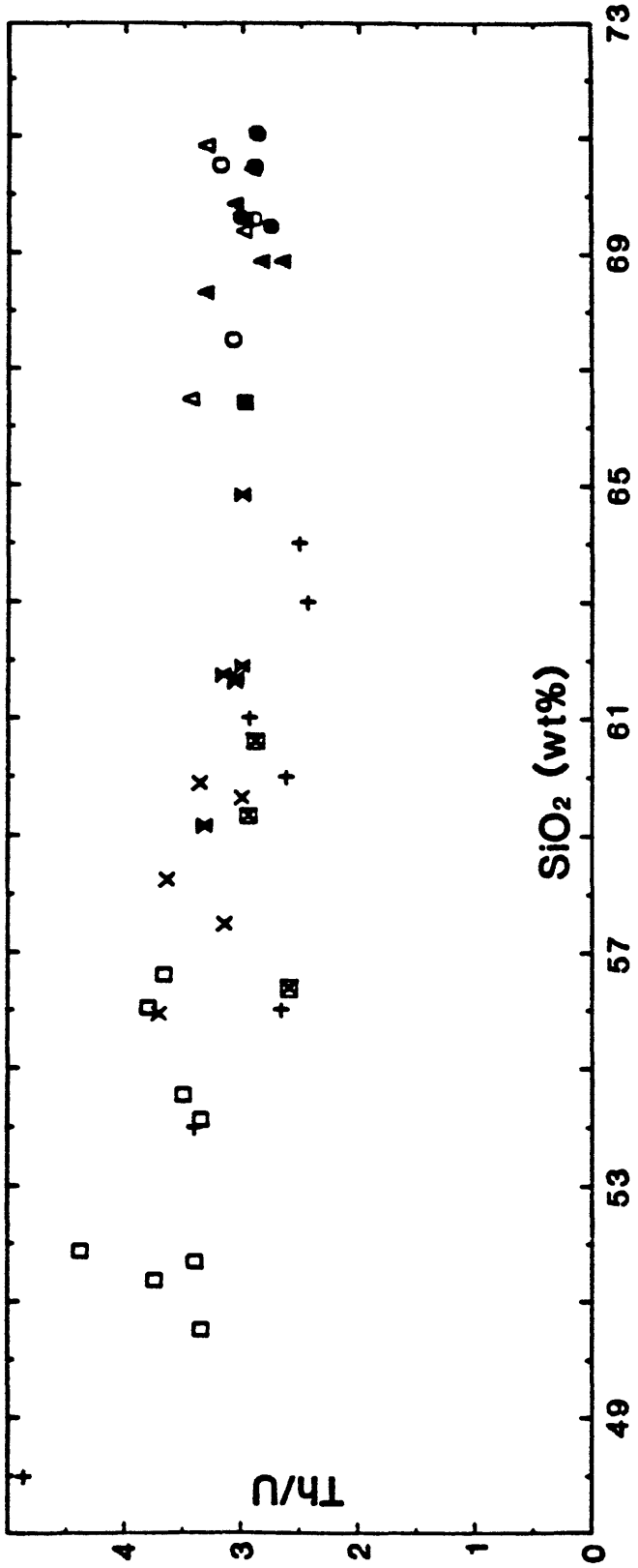

Figure 23. Th/U versus SiO2 variation diagram. Note the straight line trend with a slope of 0, indicating no change in the Th/U ratio with differentiation.

ratio can be considered to be the ratio of the primary magma. Primitive mantle has a Th/U ratio of 3.7 and a $(^{238}U/^{232}Th)$ ratio and therefore an initial $(^{230}Th/^{232}Th)_0$ ratio of 0.81 (Allegre and Condomines, 1976). Partial melting of the primitive mantle produces magmas with Th/U ratios higher than 3.7 and $(^{238}U/^{232}Th)$ ratios lower than 0.81. The rocks from the Lassen dome field have initial $(^{230}Th/^{232}Th)_0$ values greater than 0.81 suggesting that the source region for the magmas of the Lassen dome field is mantle material depeleted by a previous partial melting event (fig. 24).

This does not preclude the possibility that the magma of the Lassen dome field was produced by mixing of primitive magma (higher Th/U ratio, lower $(^{238}U/^{232}Th)$ ratio) with magma derived from parial melting of a depleted source region.

Transport of uranium in gaseous complexes, such as UF_6, upward in a magma chamber may be another explanation for the observed enrichment in thorium relative to uranium in the Lassen dome field rocks (Allegre, 1976). The Chaos Crags pyroclastic rocks (UTh-144 and UTh-145) are enriched in uranium relative to the Chaos Crags domes (UTh-83), and these samples may show the effect of gaseous transfer of uranium. Although having similar $(^{230}Th/^{232}Th)$ ratios, the dome rock (UTh-83) plots to the left of the pyroclastic rocks (UTh-144 and UTh-145), and one pyroclastic rock (UTh-145) plots to the right of the equiline (fig. 22). This indicates an enrichment of uranium relative to thorium in the pyroclastic rocks. The pyroclastic and dome rocks were rapidly erupted from the same

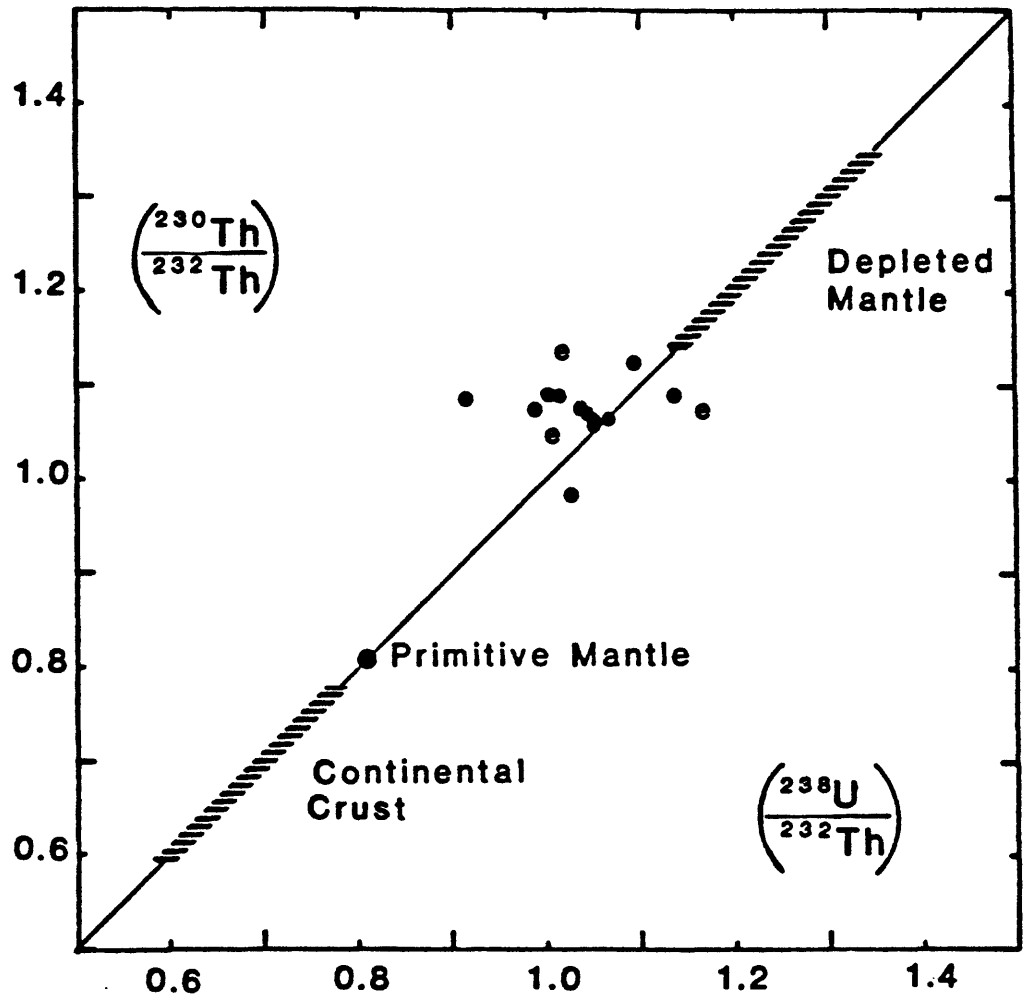

Figure 24. Isochron diagram with whole-rock data from this study plotted relative to possible magma sources for the lavas of the Lassen dome field.

magma chamber; typically the time between eruptive episodes is insufficient for fractionation processes to be operative. The pyroclastic rocks, which are enriched in uranium relative to thorium, represent the uppermost part of the magma chamber, whereas the dome rocks represent a lower zone, depleted in uranium relative to thorium.

The linear relationship shown in figure 19 suggests that the inclusions are genetically related to their host rocks. However, it is not possible at this time to explain why the Lassen Peak inclusion is enriched in uranium. A possible explanation is contamination by uranium-rich material or fractionation of uranium and thorium by some process other than partial melting. The 1915 inclusion is within error of being to the left of the equiline. In order to make a definitive statement about the mafic inclusions of the Lassen dome field, more data are needed on the inclusions, the hybrid rocks, and surrounding basalts.

CONCLUSIONS

This study is the first to obtain reliable ages on young silicic rocks using uranium-thorium disequilibrium dating tecnniques. In addition, the technique provides uranium and thorium isotopic data that can be used to assist interpretation of the evolution of magmatic systems.

Although no definitive model for the Lassen dome field is possible on the basis of data presented, some important constraints can be put on future models. The observed fractionation of thorium relative to uranium is the result of partial melting of the source material rather than fractional crystallization of the melt. The source region for the magmas of the Lassen dome field has probably been depleted by some previous partial melting event. There has been little or no assimilation of sialic crustal material and fractional crystallization is the dominant process affecting Lassen dome field magmas. Gaseous transfer of uranium-bearing complexes may be an important process of differentiation of uranium and thorium in silicic rocks in the Lassen Volcanic Center. The Lassen dome field has been active for 300,000 years and represents the third stage in the development of the Lassen Volcanic Center, which has been active for the last 600,000 years. Recent activity has produced rocks, e.g. the Chaos Crags domes and the 1915 eruption of Lassen Peak, with ($^{230}Th/^{238}U$) ratios that are not in secular

equilibrium. This indicates that the Lassen Volcanic Center is not a closed system.

The data reported here support the model of the Lassen Volcanic Center suggested by Clynne (1983). Partial melting of mantle material produces mafic magmas periodically added to the magmatic system. With time, crystal fractionation in this open system produces the continuum of intermediate to silicic compositions seen at the surface.

REFERENCES CITED

Allegre, C. J., 1968, ^{230}Th dating of volcanic rocks: A comment: Earth and Planetary Science Letters, v. 5, p. 209-210.

Allegre, C. J., and Condomines, Michel, 1976, Fine chronology of volcanic processes using ^{238}U-^{230}Th systematics: Earth and Planetary Science Letters, v. 28, p. 395-406.

Allegre, C. J., and Condomines, Michel, 1982, Basalt genesis and mantle structure studied through Th-isotopic geochemistry: Nature, v. 299, p. 21-24.

Allman, Michael, and Lawrence, D. F., 1972, Geological laboratory techniques: New York, Arco Publishing Company, Inc., 335 p.

Baranowski, J. and Harmon, R. S.,1978, U-series chronology of two rhyolites of Late Pleistocene age from Long Valley, California, in Zartman, R. E., ed., Short papers of the fourth international conference, geochronology, cosmochronology, and isotope geology, U.S. Geological Survey Open-file Report 78-71, p. 22-24.

Bateman, H., 1910, Solution of a system of differential equations occuring in the theory of radioactive transformation: Proceedings Cambridge Philisophical Society, v. 15, p. 423.

Cerrai, E., Dugnani Lonati, R., Gazzarrini, T., and Tongiorgi, E., 1965, II metodo ionio-uranio per la derterminazione dell'eta dei minerali vucanici recenti: Societa Italiana de Mineralogicae Petrologia Rendiconti, v. 21, p. 47.

Clynne, M. A., 1983, Stratigraphy and major-element geochemistry of the Lassen Volcanic Center, California: San Jose, California, San Jose State University, M.S. thesis, 167 p.

Condomines, Michel, 1978, Age of the Olby-Laschamp geomagnetic polarity event: Nature, v. 276, p. 257-258.

Condomines, Michel, and Allegre, C. J., 1980, Age and magmatic evolution of Stromboli volcano from ^{230}Th-^{238}U disequilibrium data: Nature, v. 288, p. 354-357.

Condomines, Michel, Bernat, M., and Allegre, C. J., 1976, Evidence for contamination of recent Hawaiian lavas from ^{230}Th-^{238}U data: Earth and Planetary Science Letters, v. 33, p. 122-125.

Condomines, Michel, Morand, Philippe, and Allegre, C. J., 1981a, ^{230}Th-^{238}U radioactive disequilibria in tholeiites from the FAMOUS zone (Mid-Atlantic Ridge, 36°50'N): Th and Sr isotopic geochemistry: Earth and Planetary Science Letters, v. 55, p. 247-256.

Condomines, Michel, Morand, Philippe, Allegre, C. J., and Sigvaldason, Gudmundur, 1981b, ^{230}Th–^{238}U disequilibria in historical lavas from Iceland: Earth and Planetary Science Letters, v. 55, p. 393-406.

Condomines, Michel, Tanguy, J. C., Kieffer, C., and Allegre, C. J., 1982, Magmatic evolution of a volcano studied by the ^{230}Th–^{238}U disequilibrium and trace elements systematics: the Etna case: Geochimica et Cosmochimca Acta, v. 46, p. 1397-1416.

Crandell, D. R., 1972, Glaciation near Lassen Peak, northern California: U. S. Geological Survey Professional Paper 800-C, p. C179-C188.

Crandell, D. R., Mullineaux, D. R., Sigafoos, R. S., and Rubin, Meyer, 1974, Chaos Crags eruptions and rockfall-avalanches, Lassen Volcanic National Park, California: U. S. Geological Survey Journal of Research, v. 2, p. 49-59.

Crow, E. L., Davis, F. A. and Maxfield, M. W., 1960, Statistics Manual: New York, Dover Publications, 288 p.

Deruelle, Bernard, 1982, Petrology of the Plio-Quaternary volcanism of the south-central and meridional Andes: Journal of Volcanolgy and Geothermal Research, v.14, p. 77-124.

Fountain, J. C., 1975, The geochemistry of Mt. Tehama, Lassen Volcanic National Park, California: Santa Barbara, California University of California, Ph.D. dissertation, 166 p.

Friedlander, Gerhart, Kennedy, J. W., Macia, E. S., and Miller, J.M., 1981, Nuclear and radiochemistry, 3rd ed.: New York, John Wiley and Sons, Inc., 684 p.

Fukuoka, Takaaki, 1974, Ionium dating of acidic volcanic rocks: Geochemical Journal, v. 8, p. 109-116.

Fukuoka, Takaaki, and Kigoshi, Kunihiko, 1974, Discordant Io-ages and the uranium and thorium distribution between zircon and host rocks: Geochemical Journal, v. 8, p. 117-122.

Gindler, J. E., 1962, The radiochemistry of uranium: National Academy of Sciences, Nuclear Science Series, NAS-NS 3050, 350 p.

Goldberg, E. D., and Kolde, Minoru, 1958, Ionium-thorium chronology in deep-sea sediments of the Pacific: Science, v. 128, p. 1003.

Harmon, R. S., and Rosholt, J. N., 1982, Igneous rocks, in Ivanovich, M., and Harmon, R. S., eds., Uranium series disequilibrium application to environmental problems: Oxford, Clarendon Press, 571 p.

Heiken, Grant, and Eichelberger, J. C., 1980, Eruptions at Chaos Crags, Lassen Volcanic National Park, California: Journal of Volcanology and Geothermal Research, v. 7, p. 443-481.

Hildreth, E.W., 1981, Gradients in silicic magma chambers: Implications for lithospheric magmatism: Journal of Geophysical Research, v. 86, p. 10153-10192.

Hutchison, C. S., 1974, Laboratory handbook of petrographic techniques: New York, John Wiley and Sons, 527 p.

Hyde, E. K., 1960, The radiochemistry of thorium: National Academy of Sciences, Nuclear Science Series, NAS-NS 3004, 70 p.

Kane, Phillip, 1982, Pleistocene glaciation, Lassen Volcanic National Park: California Geology, v. 35, p. 95-105.

Kelly, L. G., 1967, Handbook of numerical methods and application: Reading, Massachusetts, Addison-Wesley Publishing Co., 354 p.

Kigoshi, Kuniniko, 1967, Ionium dating of igneous rocks: Science, v. 156, p. 932-934.

Ku, T.-L., 1966, U-series disiquilibrium in deep sea sediments: New York, Columbia University, Ph.D. dissertation, 157 p.

Larsen, E. S., and Gottfried, David, 1960, Uranium and thorium in selected suites of igneous rocks: American Journal of Science, v. 258-A, p. 151-169.

Mahood, G. A., 1981, Chemical evolution of a Pleistocene rhyolitic center: Sierra La Primavera, Jalisco, Mexico: Contributions to Mineralogy and Petrology, v. 77, p. 129-149.

Newman, Sally, Finkel, R. C., and Macdougall, J. D., 1981, ^{238}U-^{230}Th systematics of young volcanics: EOS, v. 62, p. 1076.

Taddeucci, Adriano, Broecker, W. S., and Thurber, D. L., 1967, ^{230}Th dating of volcanic rocks: Earth and Planetary Science Letters, v. 3, p. 338-342.

Tatsumoto, Mitsunobu, 1978, Isotopic composition of lead in oceanic basalt and its implication to mantle evolution: Earth and Planetary Science Letters, v. 38, p. 63-87.

Taylor, S. R., and White, A. J. R., 1966, Trace element abundances in andesites: Bulletin Volcanologique, v. 29, p. 177-194.

Thurber, D. L., 1963, Anomalous $^{234}U/^{238}U$ and an investigation of the potential of ^{234}U for Pleistocene chronology: New York, Columbia University, Ph.D. dissertation, 165 p.

Weast, R. C., ed., 1979, Handbook of chemistry and physics: Boca Raton, Florida, Chemical Rubber Publishing Company, 2446 p.

Williams, Howel, 1932, Geology of the Lassen Volcanic National Park, California: University of California, Department of Geological Sciences Bulletin, v. 21, p. 195-385.

York, Derek, 1967, The best isochron: Earth and Planetary Science Letters, v. 2, p. 479-482.

York, Derek, 1969, Least squares fitting of a straight line with correlated errors: Earth and Planetary Science Letters, v. 5, p. 320-324.

APPENDIX 1: CHEMISTRY FLOW CHART

	Precipitate	Solution
NH_4OH	U, Th Fe, Al, Ni, Ti, Zr Some REE, Cr, Mo, Cu, Zn, Sc	Na, K, Mg, Ca, Mn, Li Rb, Cs, Ba, Be, Ra
3N NaOH Wash	U, Th Fe, Ni, Ti, Zr Some REE, Cr, Mo Cu, Zn, Sc	Al

	Extracted	Not Extracted
Ether Extraction	Fe	All other elements present

	Absorbed	Not Absorbed
Anion Exchange AG 1X8 8N HCl	U, Fe, Zr,Cr, Nb, Mo, V, Cu	Th, REE, Ni, Sc, Rb, Y, Li, Ti(?)
Anion Exchange AG 1X8 8N HNO_3	U, Th	Fe, Cr, V, Cu, Zr( ) Mo(?), Nb(?)

	pH = 1 to 2	pH = 3 to 4
TTA Purification	Th	U

APPENDIX 2: LOCATION OF SAMPLES IN TABLES 5 AND 6

Sample Number	Latitude North	Longitude West	Locality Description
UTh-62	40°30.72'	121°29.92'	NW side of Crescent Crater
UTh-64	40°28.62'	121°30.51'	West of Lassen Peak Trail Parking Lot
UTh-80	40°28.36'	121°30.25'	LVNP Road east of Lake Helen
UTh-83	40°32.56'	121°32.31'	Chaos Crags dome 3 of Crandall and others, 1974
UTh-84	40°30.58'	121°24.65'	NW of Summit of Hill 7263'
UTh-113	40°29.35'	121°30.25'	1915 Flow, summit Lassen Peak
UTh-121	40°28.36'	121°30.25'	LVNP road east of Lake Helen
UTh-122	40°30.11'	121°33.92'	West end of Loomis Peak
UTh-129	40°29.23'	121°30.47'	1915 Flow, summit Lassen Peak
UTh-134	40°28.62'	121°30.51'	West of Lassen Peak Trail Parking Lot
UTh-142	40°28.23'	121°29.48'	LVNP road west of Reading Peak
UTh-143	40°31.65'	121°34.53'	Junction CA Highways 89 and 44
UTh-144	40°31.69'	121°29.09'	Sand Pit Quarry, Lost Creek
UTh-145	40°30.42'	121°30.93'	LVNP Quarry, Manzanita Creek
UTh-150	40°33.40'	121°31.77'	Sunflower Flat